Radboud Universiteit

Structural commensurability and incommensurability in twisted Van der Waals systems

Mikhail Katsnelson

IMM
Institute for Molecules and Materials

Outline

I. Van der Waals heterostructures: Introduction
II. Phase synchronization and commensurate – incommensurate transition in general
III. Graphene on hBN: (1) atomic reconstruction; (2) effect on electronic structure; (3) transport; (4) nonlinear optics
IV. Graphene on graphite and/or twisted bilayer graphene: (1) atomic reconstruction and vortex lattice formation; (2) description in terms of misfit dislocations; (3) pseudomagnetic field and electronic structure

Zoo of 2D materials

Plenty of 2D materials starting from graphene

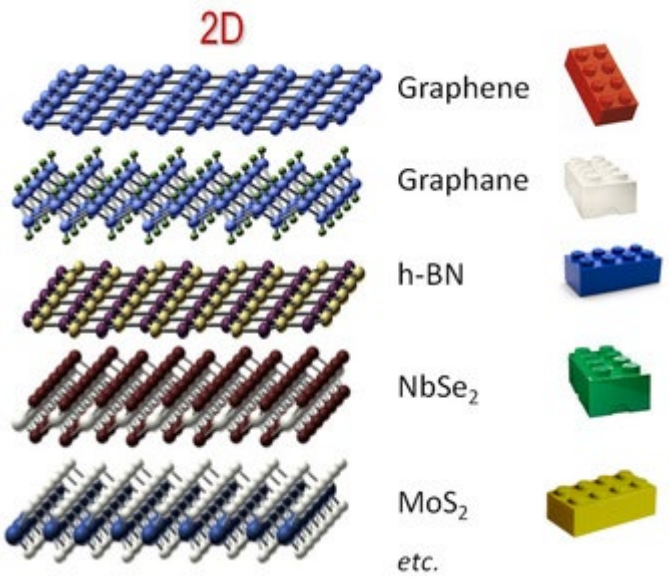

Semimetals (graphene), semiconductors, metals, superconductors, broad-gap insulators...

Graphene

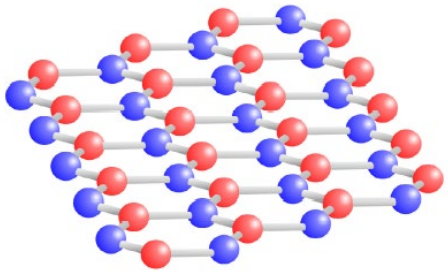

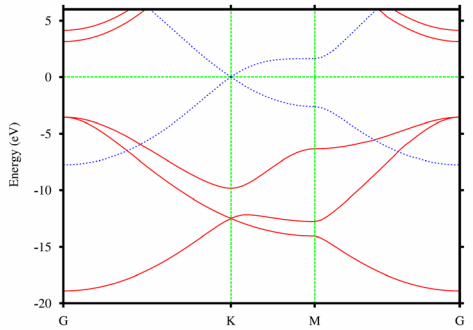

FIG. 2: (color online) Band structure of a single graphene layer. Solid red lines are σ bands and dotted blue lines are π bands.

Silicene, germanene

Buckling

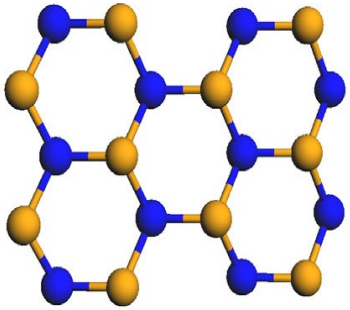

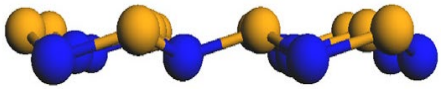

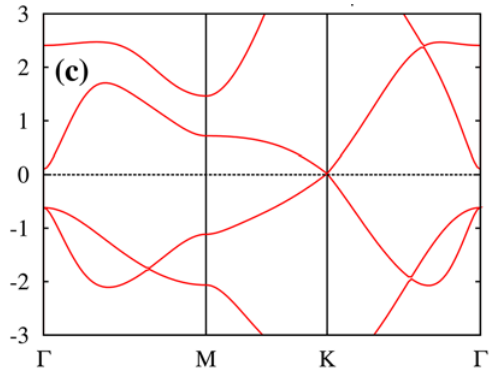

OPEN ACCESS
IOP Publishing
Journal of Physics: Condensed Matter

J. Phys.: Condens. Matter **27** (2015) 443002 (11pp)
doi:10.1088/0953-8984/27/44/443002

Topical Review

Germanene: the germanium analogue of graphene

A Acun[1,6], L Zhang[1,6], P Bampoulis[1], M Farmanbar[2], A van Houselt[1], A N Rudenko[3], M Lingenfelder[4,5], G Brocks[2], B Poelsema[1], M I Katsnelson[3] and H J W Zandvliet[1]

Zoo of 2D materials - semiconductors

Antimony

PHYSICAL REVIEW B **95**, 081407(R) (2017)

Electronic properties of single-layer antimony: Tight-binding model, spin-orbit coupling, and the strength of effective Coulomb interactions

A. N. Rudenko,[1,*] M. I. Katsnelson,[1] and R. Roldán[2]

The same buckled structure as for silicene or germanene

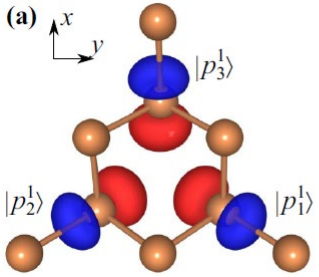

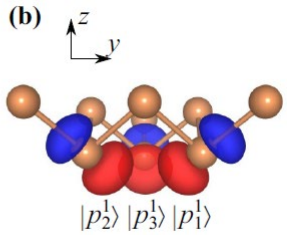

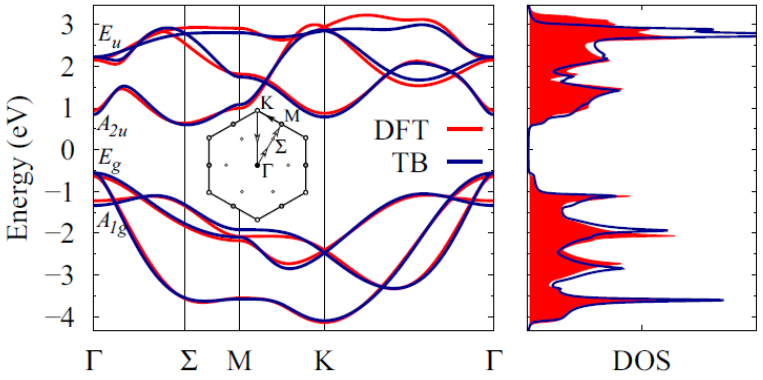

Strong spin-orbit coupling $\lambda = 0.34$ eV

InSe

PHYSICAL REVIEW LETTERS **123,** 176401 (2019)

Strong Electron-Phonon Coupling and its Influence on the Transport and Optical Properties of Hole-Doped Single-Layer InSe

A. V. Lugovskoi,[1] M. I. Katsnelson,[1,2] and A. N. Rudenko[3,1,2,*]

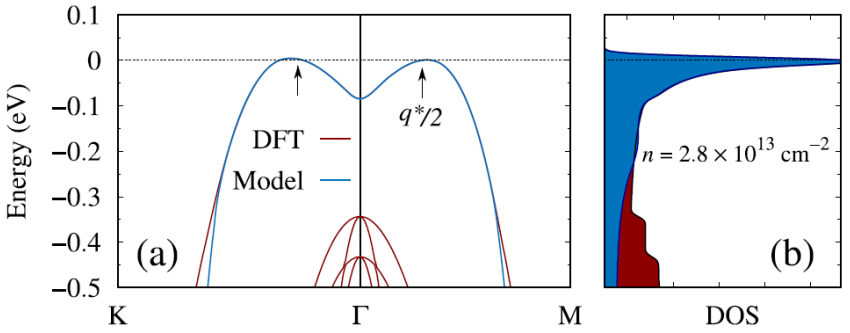

Flat band, strong elctron-phonon coupling

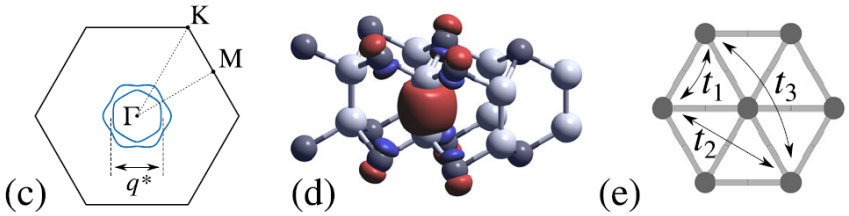

Zoo of 2D materials – Magnetic materials

CrX_3

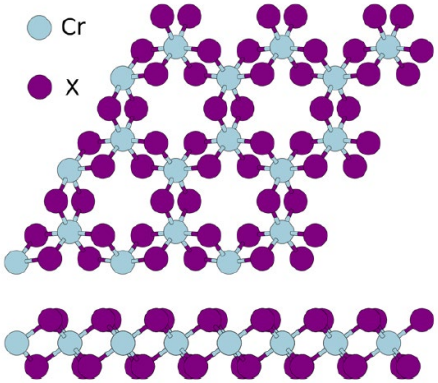

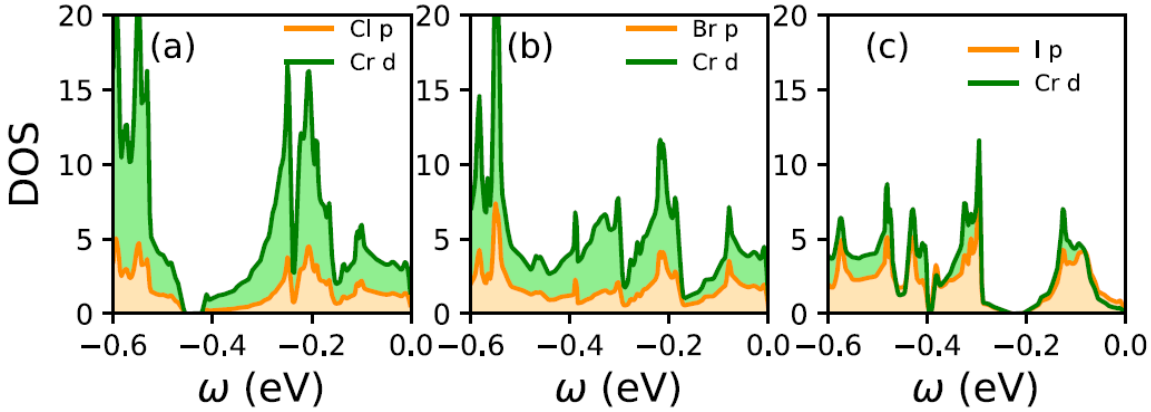

CrSBr (highly anisotropic)

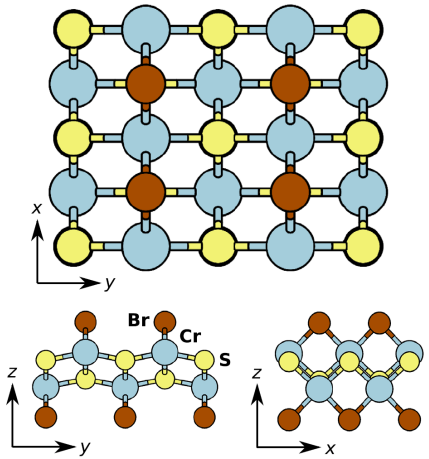

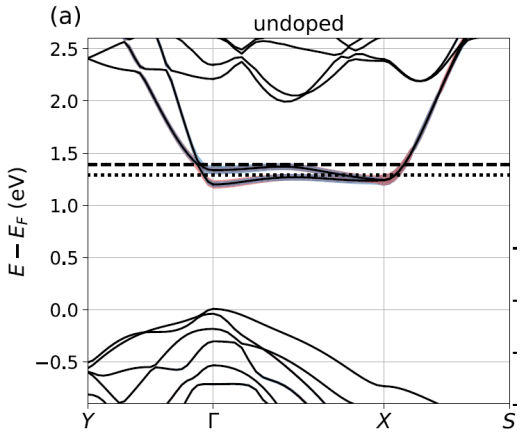

Fe_3GeTe_2 (metallic)

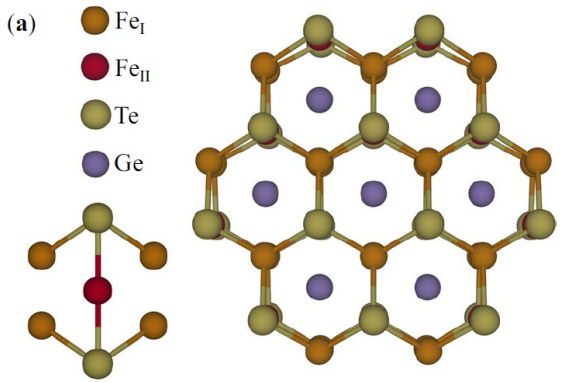

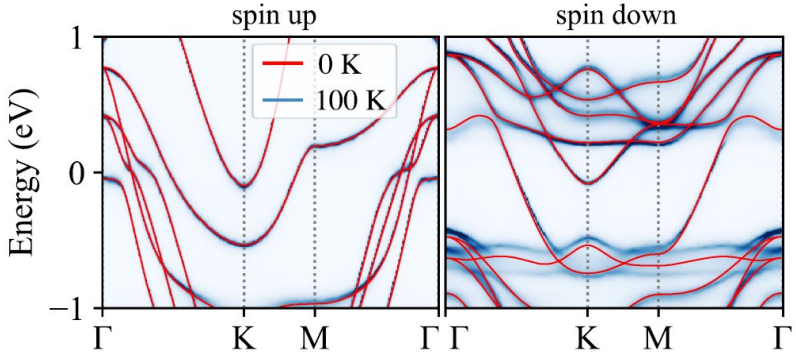

Van der Waals Heterostructures

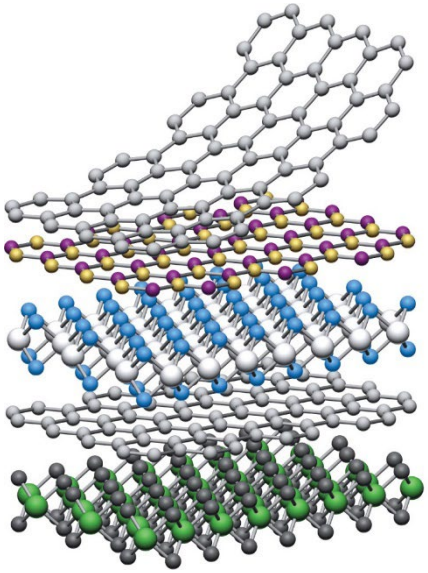

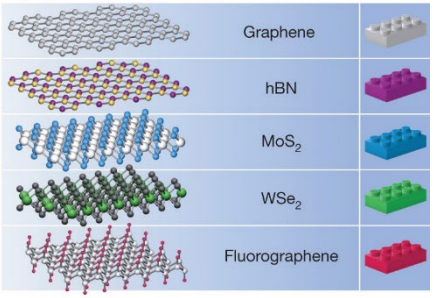

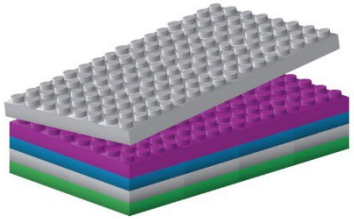

"Van der Waals heterostructures"
Geim & Grigorieva, Nature 2013

Combination of 2D materials create new physical systems and open ways for new application

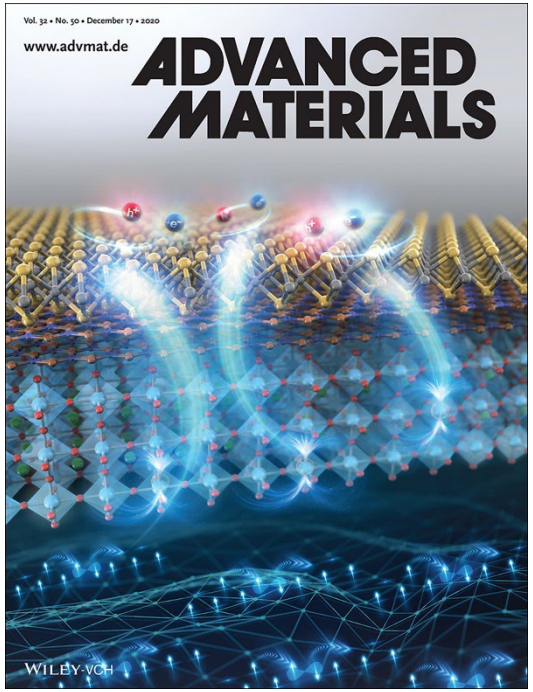

Twisted bilayer graphene: Flat bands and all that

Correlated insulator behaviour at half-filling in magic-angle graphene superlattices

Yuan Cao[1], Valla Fatemi[1], Ahmet Demir[1], Shiang Fang[2], Spencer L. Tomarken[1], Jason Y. Luo[1], Javier D. Sanchez-Yamagishi[2], Kenji Watanabe[3], Takashi Taniguchi[3], Efthimios Kaxiras[2,4], Ray C. Ashoori[1] & Pablo Jarillo-Herrero[1]

Unconventional superconductivity in magic-angle graphene superlattices

Yuan Cao[1], Valla Fatemi[1], Shiang Fang[2], Kenji Watanabe[3], Takashi Taniguchi[3], Efthimios Kaxiras[2,4] & Pablo Jarillo-Herrero[1]

5 APRIL 2018 | VOL 556 | NATURE | 43

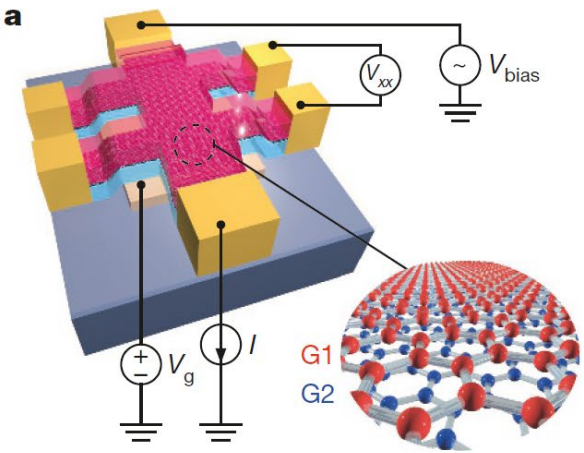

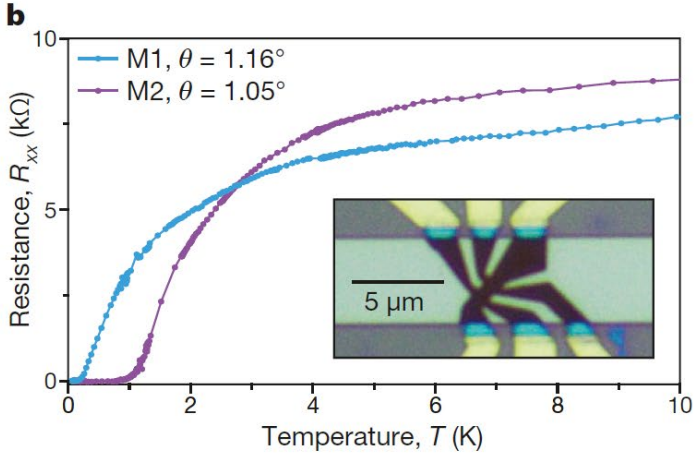

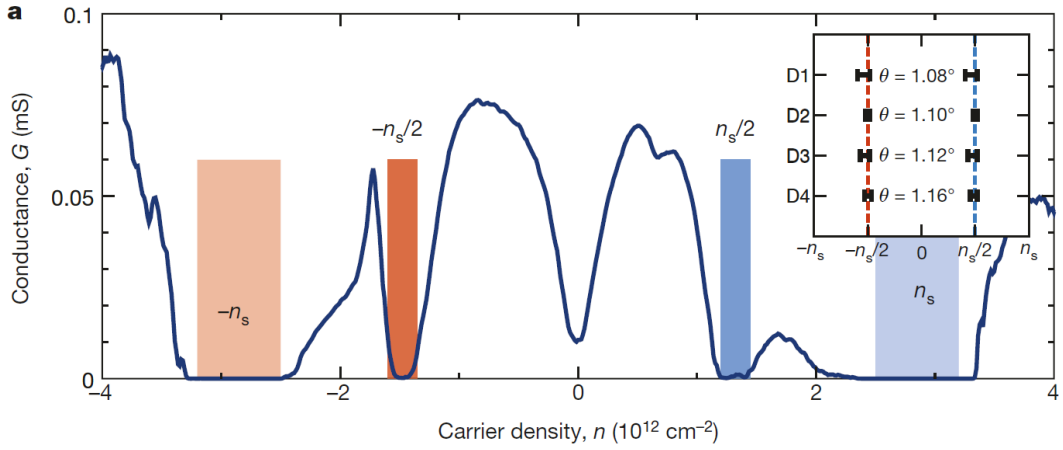

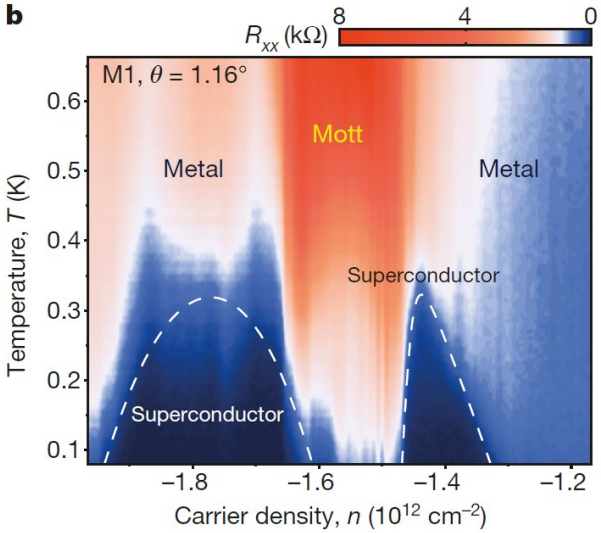

Example: Graphene on hBN

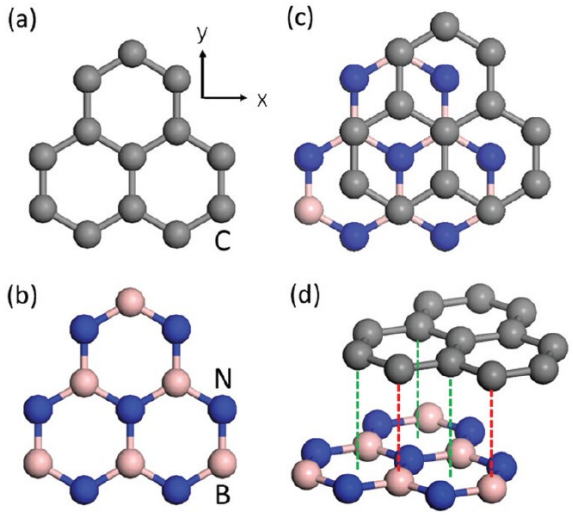

Chen & Qin, JPCC 8, 12085 (2020)

Graphene and hexagonal boron nitride (hBN) have the same crystal structure but slightly different interatomic distances (roughly, 0.142 nm vs 0.145 nm). In hBN they are 1.8% larger

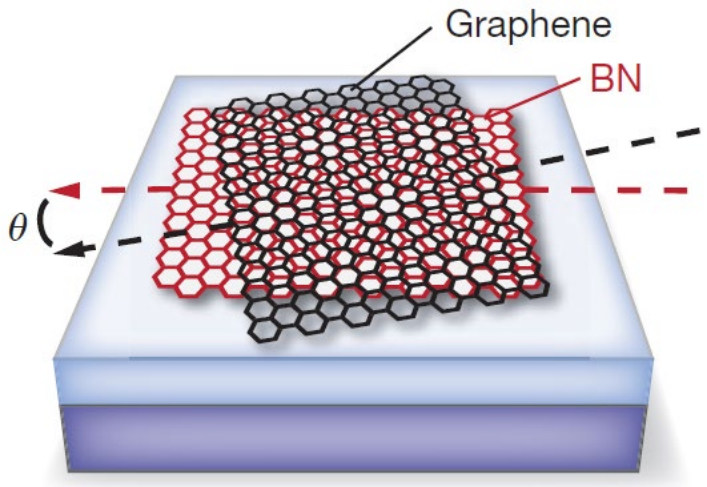

Dean et al, Nature 497, 598 (2013)

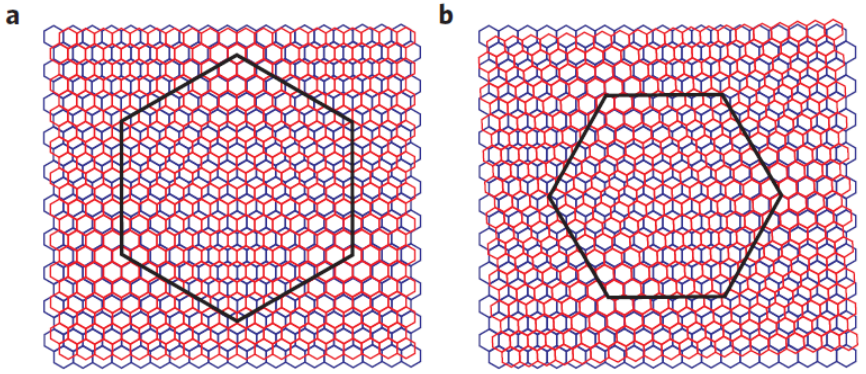

Figure 1 | Schematic representation of the moiré pattern of graphene (red) on hBN (blue). a Relative rotation angle between the crystals $\varphi = 0°$. **b** Relative rotation angle between the crystals $\varphi = 3° \approx 0.052$ rad. The mismatch between the lattices is exaggerated (~10%). Black hexagons mark the moiré plaquette.

Woods et al, Nature Phys. 10, 451 (2014)

Graphene on hBN: Motivation

Graphene at hBN has much higher electron mobility than graphene at any other substrates or freely suspended graphene – why?

Ripples and puddles

Freely suspended graphene has strong thermal fluctuations (intrinsic ripples)

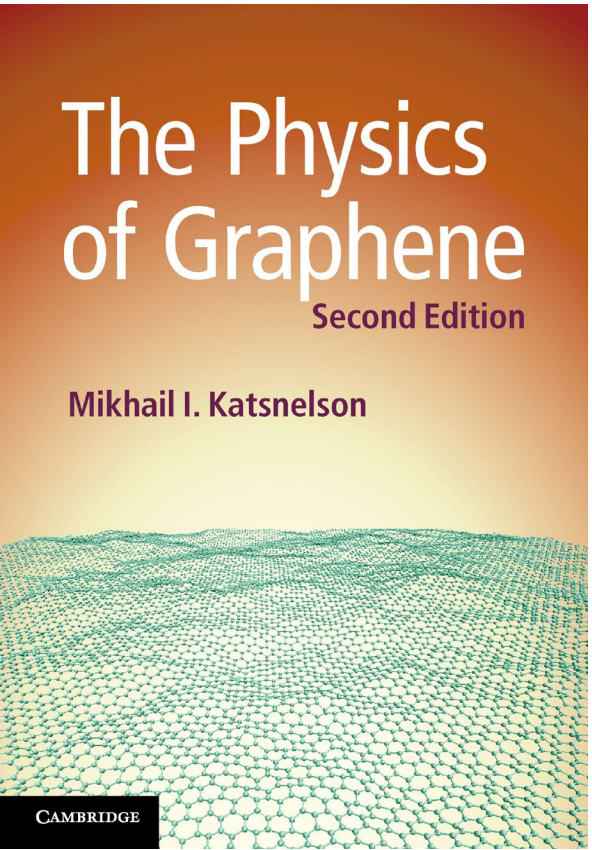

Gibertini, Tomadin, Polini, Fasolino & MIK, PR B81, 125437 (2010)

Atomic displacements at room temperature

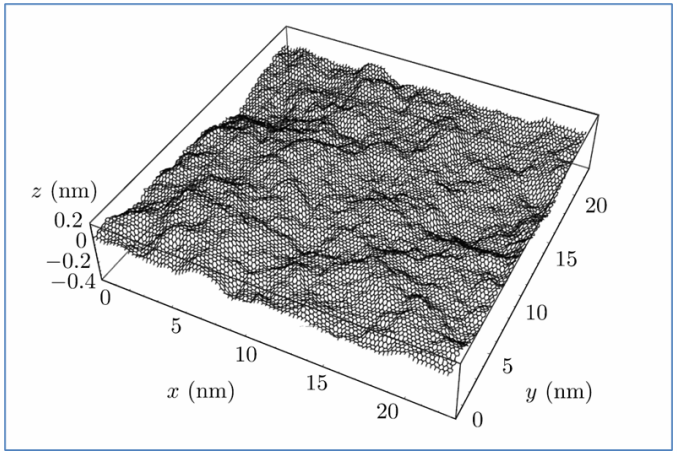

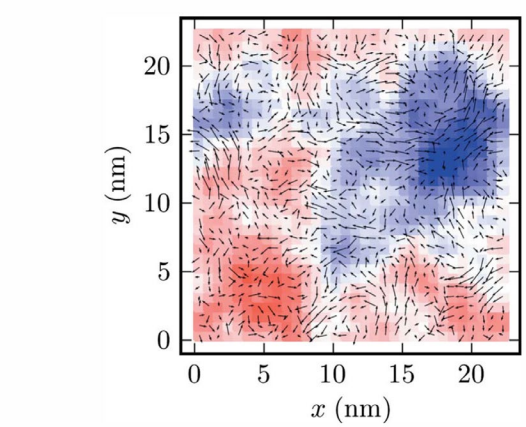

FIG. 2. (Color online) Average displacements $\overline{u}(r)$ calculated as discussed in Sec. II A. The color scale represents the $\hat{z}$ component of the average displacements, varying from −3.0 Å (blue) to +3.0 Å (red). The arrows, whose length has been multiplied by a factor ten for better visibility, represent the in-plane components of the average displacements.

Graphene on hBN: Motivation II

Scalar potential

$$V_1 = g_1(u_{xx} + u_{yy})$$

Vector potential

$$V_2 = g_2(u_{xx} - u_{yy} + 2iu_{xy})$$

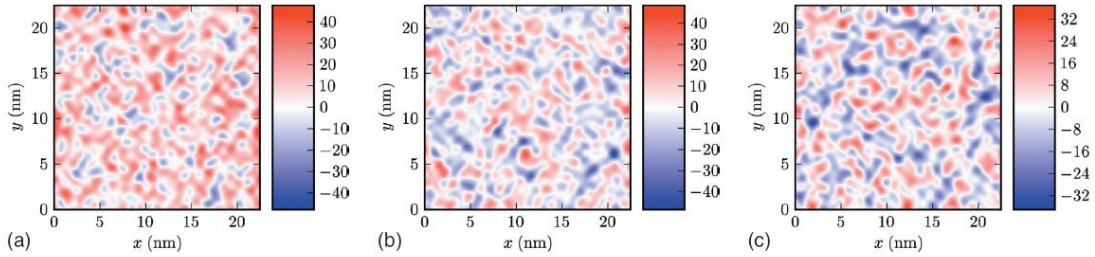

FIG. 3. (Color online) Left panel: color plot of the scalar potential $V_1(\boldsymbol{r})$ (in units of meV) calculated using Eq. (2) with g_1=3 eV. Central panel: the real part of the potential $V_2(\boldsymbol{r})$ (in units of meV) calculated using Eq. (3). Right panel: the imaginary part of the potential $V_2(\boldsymbol{r})$ (in units of meV).

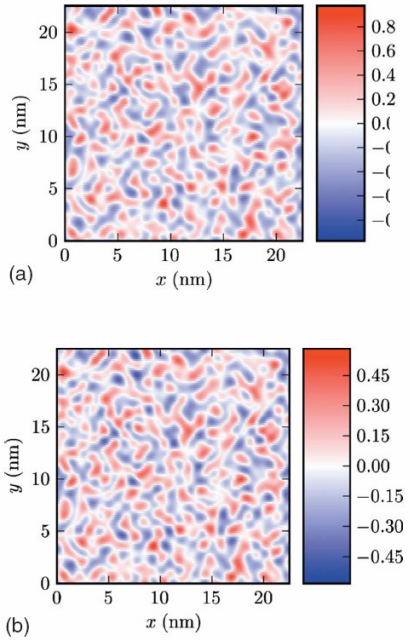

FIG. 4. (Color online) Top panel: fully self-consistent electronic density profile $\delta n(\boldsymbol{r})$ (in units of 10^{12} cm^{-2}) in a corrugated graphene sheet. The data reported in this figure have been obtained by setting g_1=3 eV, α_{ee}=0.9 (this value of α_{ee} is the commonly used value for a graphene sheet on a SiO_2 substrate), and an average carrier density $\bar{n}_c \simeq 0.8 \times 10^{12}$ cm^{-2}. Bottom panel: same as in the top panel but for α_{ee}=2.2 (this value of α_{ee} corresponds to suspended graphene).

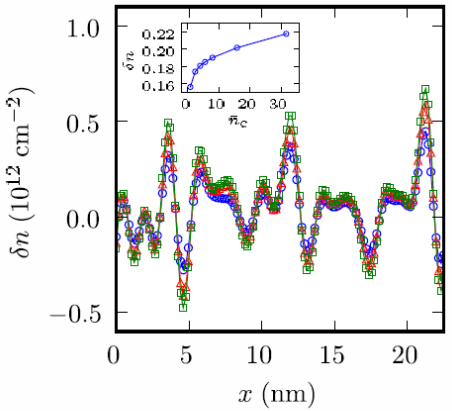

FIG. 9. (Color online) One-dimensional plots of the self-consistent density profiles (as functions of x in nm for y=21.1 nm) for different values of doping: $\bar{n}_c \simeq 0.8 \times 10^{12}$ cm^{-2} (circles), $\bar{n}_c \simeq 3.96 \times 10^{12}$ cm^{-2} (triangles), and $\bar{n}_c \simeq 3.17 \times 10^{13}$ cm^{-2} (squares). The data reported in this figure have been obtained by setting g_1=3 eV and α_{ee}=2.2. The inset shows $\delta n(\boldsymbol{r})$ (in units of 10^{12} cm^{-2}) at a given point $\boldsymbol{r}$ in space as a function of the average carrier density $\bar{n}_c$ (in units of 10^{12} cm^{-2}).

Graphene on hBN: Motivation III

Graphene on SiO_2

Gibertini, Tomadin, Guinea, MIK & Polini PR B 85, 201405 (2012)
Experimental STM data: V.Geringer et al (M.Morgenstern group)

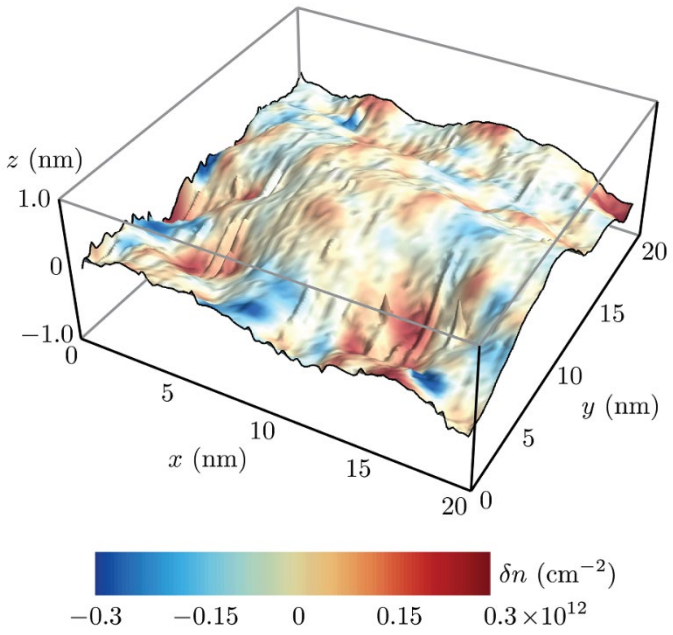

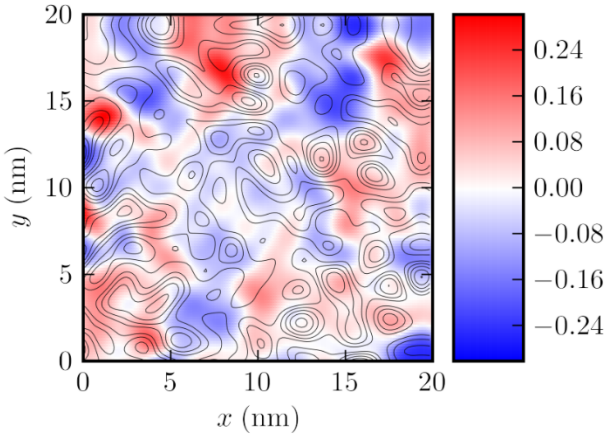

FIG. 3: (Color online) Fully self-consistent induced carrier-density profile $\delta n(\boldsymbol{r})$ (in units of 10^{12} cm^{-2}) in the corrugated graphene sheet shown in Fig. 1. The data reported in this figure have been obtained by setting $g_1 = 3$ eV, $\alpha_{ee} = 0.9$, and an average carrier density $\bar{n}_c \approx 2.5\times10^{11}$ cm^{-2}. The thin solid lines are contour plots of the curvature $\nabla^2_{\boldsymbol{r}} h(\boldsymbol{r})$. Note that there is no simple correspondence between topographic out-of-plane corrugations and carrier-density inhomogeneity.

hBN is atomically flat: suppresses thermal ripples and no ripples due to roughness of substrate

Phase locking (synchronization)

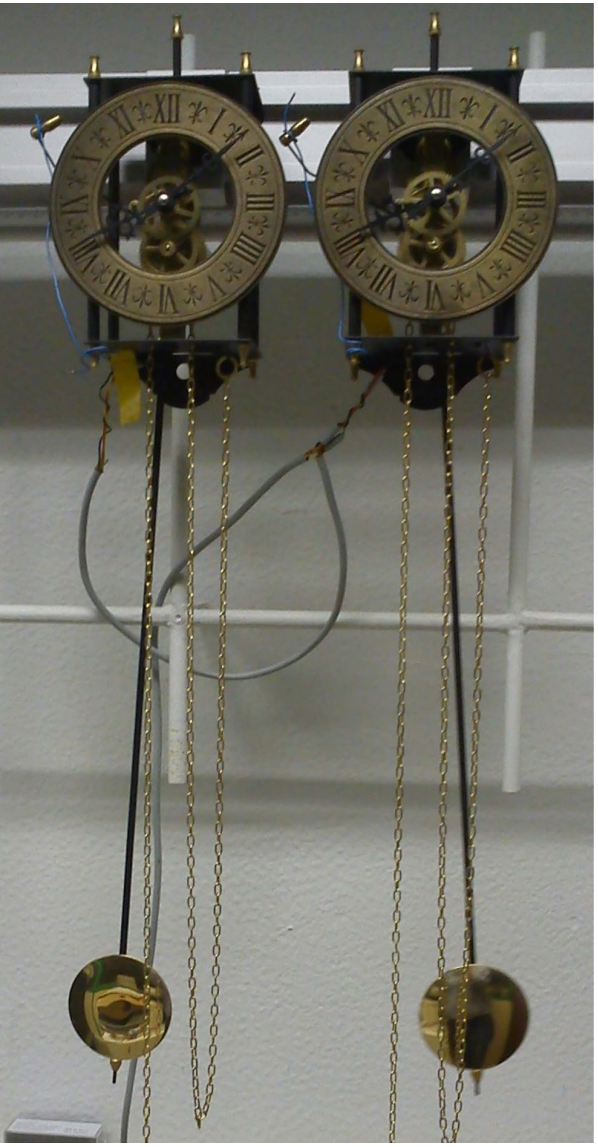

Oliveira & Melo, Sci Rep 2015

Discovered by Huygens, XVII century)

If you have two coupled oscillators with slightly different frequencies they can be synchronized

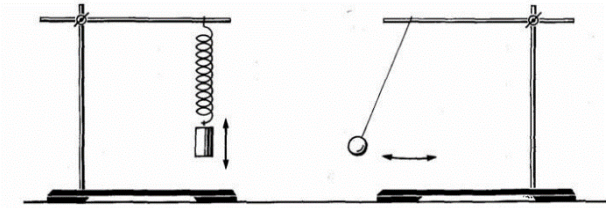

E.g., string pendulum, frequency ratio close to 1:2

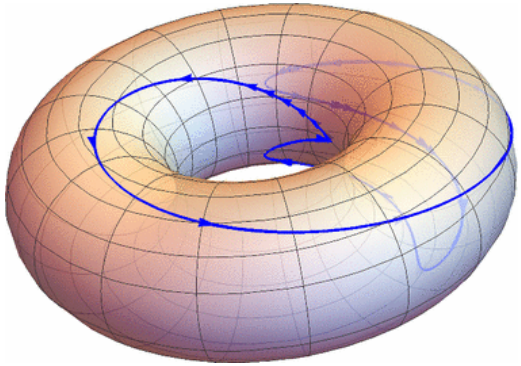

Llibre et al, J. Dyn. Dif. Eq. (2018)

Bifurcation of torus (with two incommensurate frequencies) into limit circle (with one common period)

Phase locking (synchronization) II

Resonance phenomena in a phonon subsystem in connection with anomalies of the structural state of metals

M. I. Katsnel'son and A. V. Trefilov
I. V. Kurchatov Institute of Atomic Energy, Moscow; Institute of Metal Physics, Ural Science Center, Academy of Sciences of the USSR

(Submitted 2 April 1987)
Pis'ma Zh. Eksp. Teor. Fiz. **45**, No. 10, 496–498 (25 May 1987)

Hypothesis on the role of phonon phase locking in development of structural instabilities (including melting) in solids

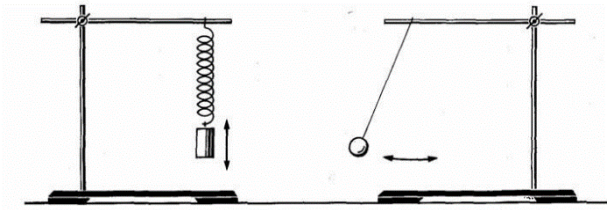

String pendulum, frequency ratio close to 1:2

Stochastic resonance between limit cycles. Spring pendulum in a thermostat

Yu. N. Gornostyrev, D. I. Zhdakhin, and M. I. Katsnel'son
Institute of Metal Physics, Ural Branch of the Russian Academy of Sciences, 620219 Ekaterinburg, Russia

A. V. Trefilov
Russian Science Center "Kurchatov Institute," 123182 Moscow, Russia

(Submitted 18 March 1999)
Pis'ma Zh. Éksp. Teor. Fiz. **69**, No. 8, 585–589 (25 April 1999)

Two limit circles with different total phases and thermally induced transitions between them

$$s(t)=\Omega_0\int_{t-n\pi/\Omega_0}^{t+n\pi/\Omega_0} x^2(t')y(t')\cos(4\Omega_0 t')dt'$$

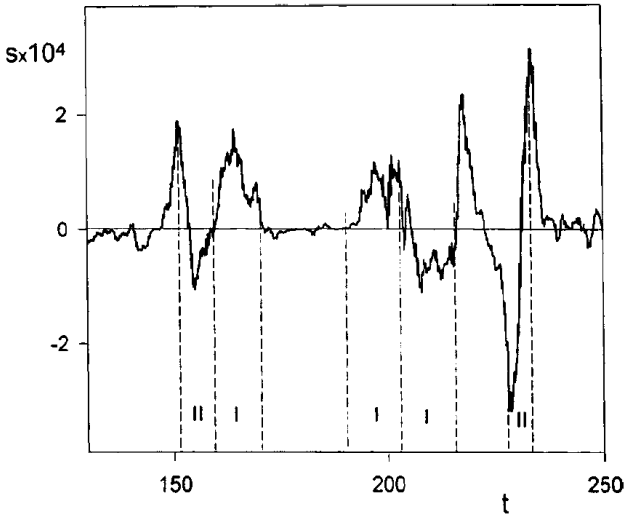

FIG. 2. $s(t)$ (see the expression (4)) for the same parameters as in Fig. 1. The sections corresponding to phase synchronization (limit cycles) are designated by I, and the sections corresponding to fast transitions between limit cycles are designated by II.

Misfit dislocations

One-dimensional dislocations.
I. Static theory

By F. C. Frank and J. H. van der Merwe
H. H. Wills Physical Laboratory, University of Bristol

(*Communicated by N. F. Mott, F.R.S.—Received 22 December 1948—Revised 25 March 1949—Read 19 May 1949*)

$$V_N = \tfrac{1}{2}\mu \sum_{n=0}^{N-1} (x_{n+1} - x_n + a - b)^2 + \tfrac{1}{2}W \sum_{n=0}^{N-1} (1 - \cos 2\pi x_n/a)$$

Energy of interlayer interaction (second term) wants that interatomic distances are equal but then one pays for the energy of elastic deformation (the first term)

Interface of different semiconductors (e.g. PbTe/PbSe)

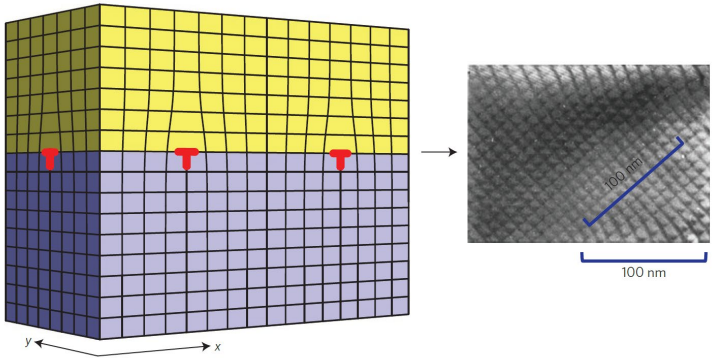

Tang & Fu, Nature Phys. 10, 964 (2014)

Very roughly: When $W > \mu(b-a)^2$ then two layers will be mostly commensurate, and the whole misfit will be concentrated via narrow 'solitons', and in the opposite limit the system will not even try To reach synchronization of periods, that is, commensurability

Commensurate – incommensurate transition is expected!

Commensurate-incommensurate transition

Commensurate–incommensurate transition in graphene on hexagonal boron nitride

C. R. Woods[1], L. Britnell[1], A. Eckmann[2], R. S. Ma[3], J. C. Lu[3], H. M. Guo[3], X. Lin[3], G. L. Yu[1], Y. Cao[4], R. V. Gorbachev[4], A. V. Kretinin[1], J. Park[1,5], L. A. Ponomarenko[1], M. I. Katsnelson[6], Yu. N. Gornostyrev[7], K. Watanabe[8], T. Taniguchi[8], C. Casiraghi[2], H-J. Gao[3], A. K. Geim[4] and K. S. Novoselov[1]*

NATURE PHYSICS DOI: 10.1038/NPHYS2954

When misorientation angle (in radians) is smaller with misfit, synchronization happens

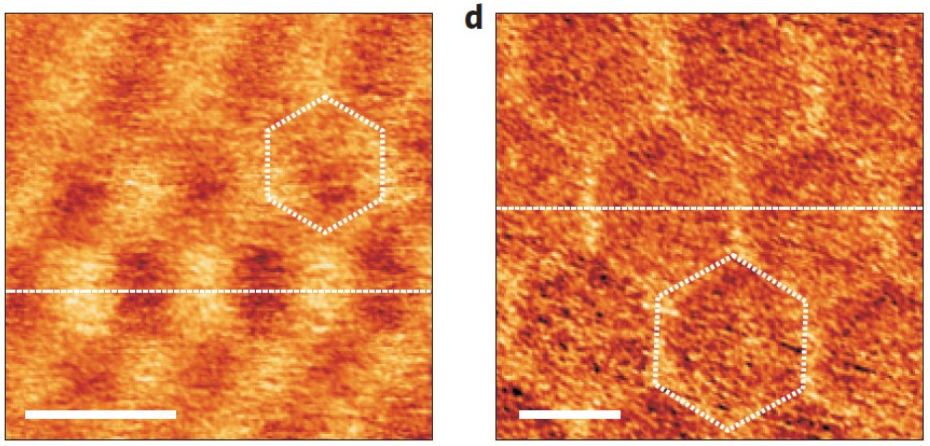

Moire patterns with periodicity 8 nm (left) and 14 nm (right)

Atomistic simulations

PRL 113, 135504 (2014) PHYSICAL REVIEW LETTERS week ending 26 SEPTEMBER 2014

Moiré Patterns as a Probe of Interplanar Interactions for Graphene on h-BN

M. M. van Wijk, A. Schuring, M. I. Katsnelson, and A. Fasolino*

Distribution of bond length in commensurate (left) and incommensurate (right) regimes

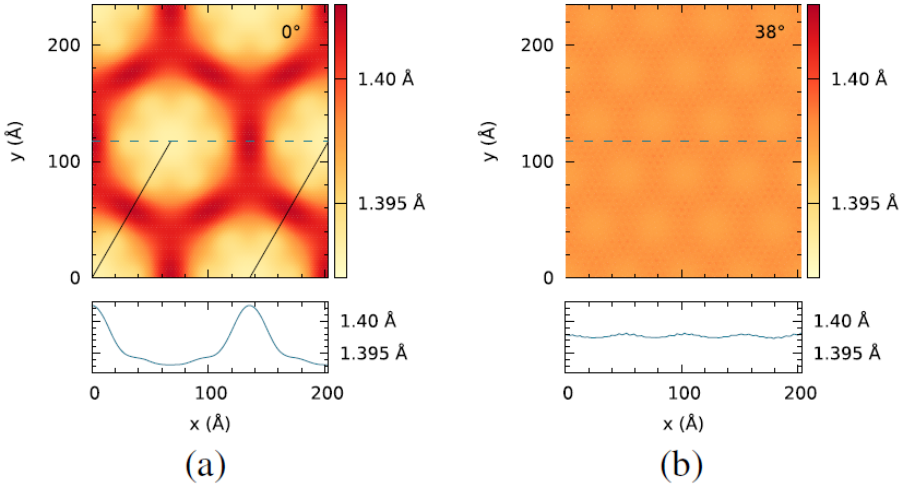

Consequences for electronic structure

PHYSICAL REVIEW B **84**, 195414 (2011)

Adhesion and electronic structure of graphene on hexagonal boron nitride substrates

B. Sachs,[1,*] T. O. Wehling,[1,†] M. I. Katsnelson,[2] and A. I. Lichtenstein[1]

Relaxed structure (B green, C yellow, N red)

V corresponds to the minimal energy (max. cohesion)

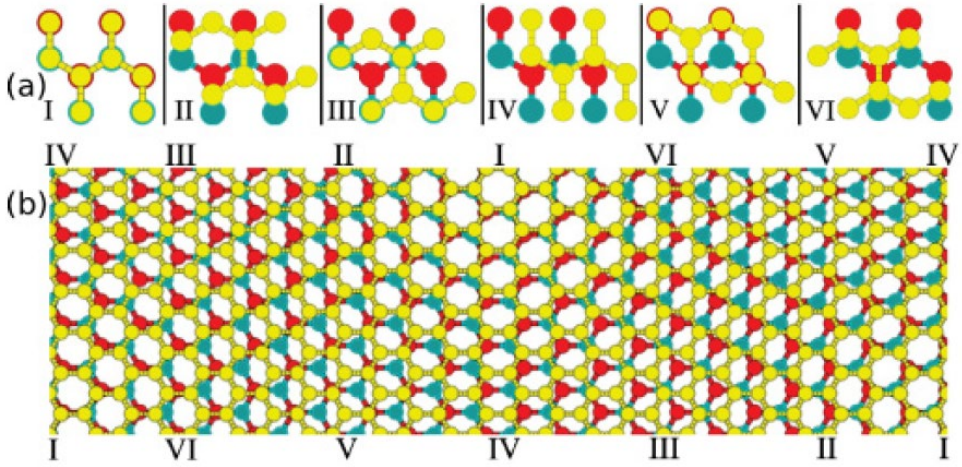

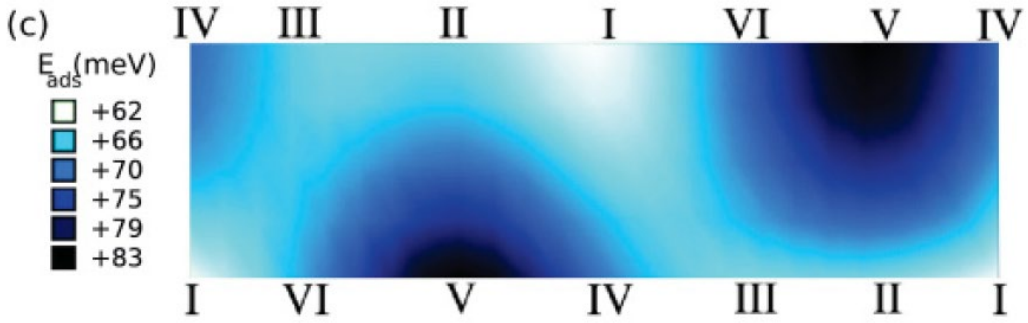

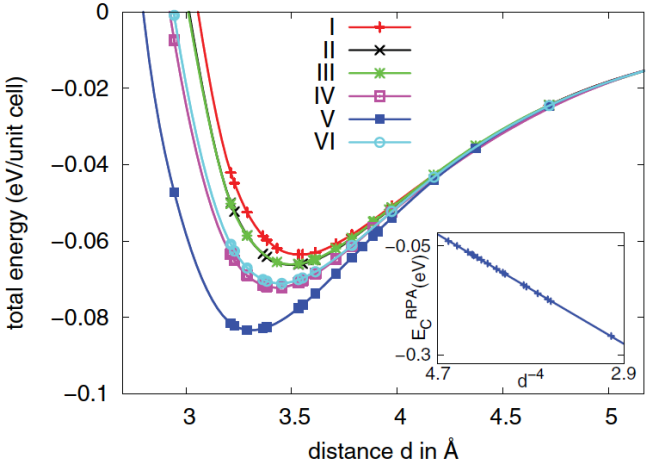

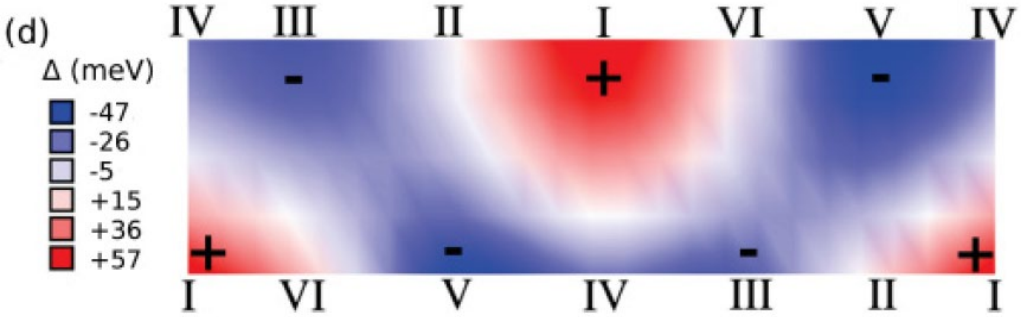

B on the top of C, N in the middle of hexagon
Sublattices are no more equivalent → locally energy gap is open (mass term in Dirac eq.)

Consequences for electronic structure II

PRL 115, 186801 (2015) PHYSICAL REVIEW LETTERS week ending 30 OCTOBER 2015

Effect of Structural Relaxation on the Electronic Structure of Graphene on Hexagonal Boron Nitride

G. J. Slotman,[1] M. M. van Wijk,[1] Pei-Liang Zhao,[2] A. Fasolino,[1] M. I. Katsnelson,[1] and Shengjun Yuan[1,*]

Atomic relaxation in commensurate phase modulates the Hamiltonian parameters

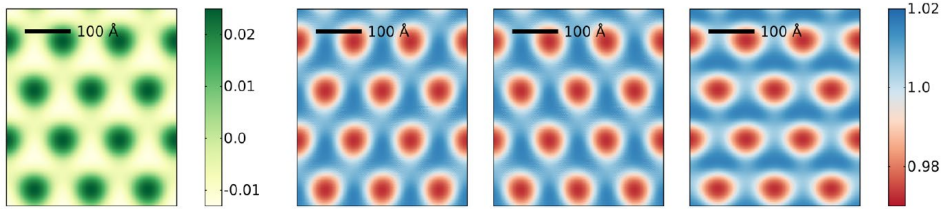

FIG. 1 (color online). The modified TB parameters for a relaxed sample of graphene on hBN with $\theta = 0°$ ($\lambda = 13.8$ nm). From left to right, the on-site potential v and the hopping parameters t_1, t_2, and t_3. The color bars are in units of $t = 2.7$ eV.

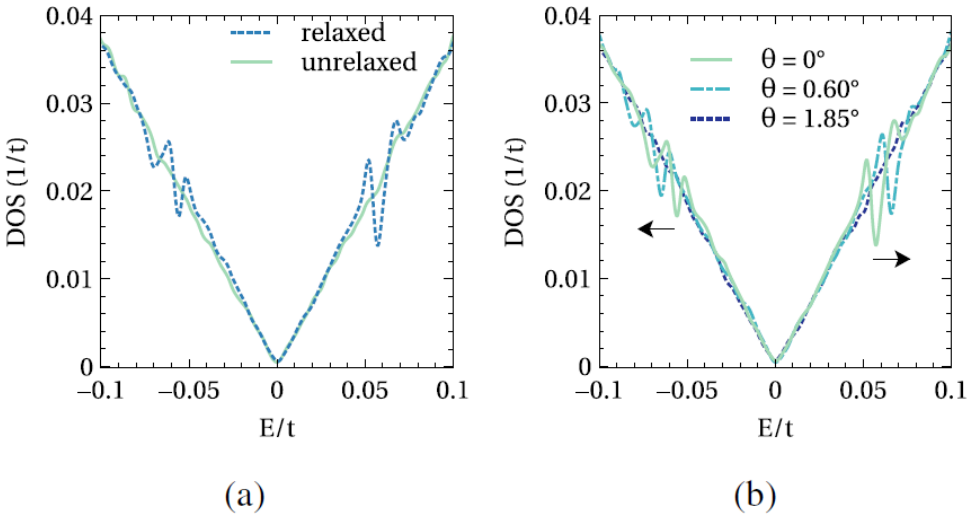

Very strong effect of atomic relaxation!

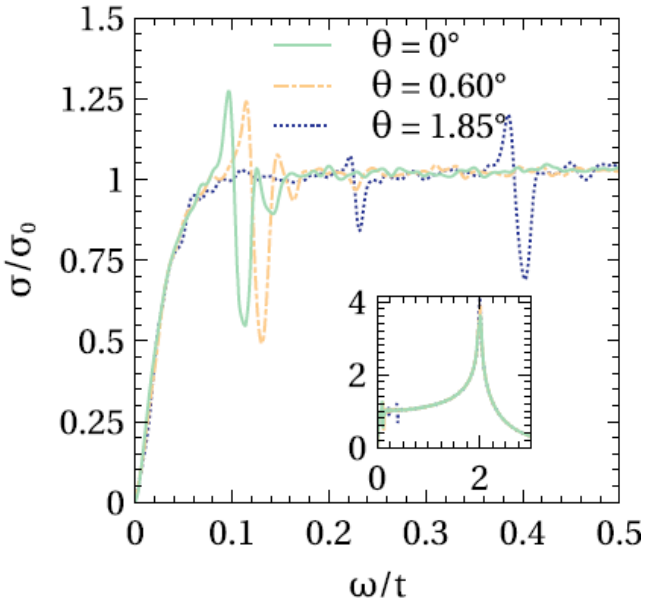

Optical conductivity

Consequences for electronic transport

In commensurate phase average gap is non zero, and system can be insulating

For incommensurate phase, the average gap is zero, and there are electron states along zero-mass lines
Tudorovskiy & MIK, PRB **86**, 045419 (2012)

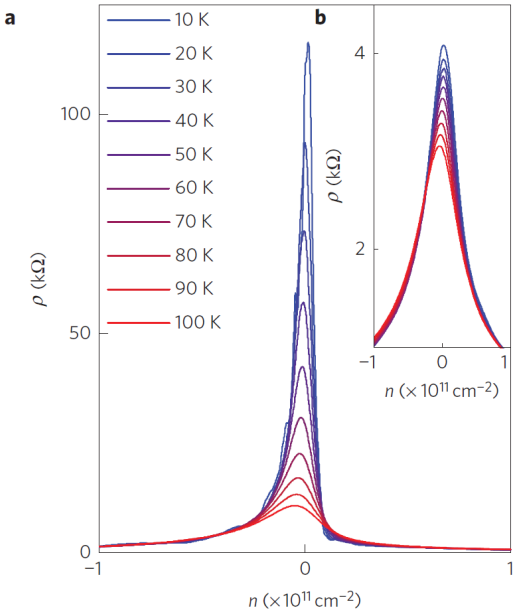

Woods et al, Nature Phys. 10, 451 (2014)

Straight zero-mass line (y =0): $\hat{H} = \sigma_x \hat{p}_x + \sigma_y \hat{p}_y + \sigma_z m(y)$

$$\Psi = e^{ip_x x}\chi(y) \qquad \chi = \frac{1}{\sqrt{2}}\begin{pmatrix}1\\1\end{pmatrix}\eta_1 + \frac{1}{\sqrt{2}}\begin{pmatrix}1\\-1\end{pmatrix}\eta_2$$

Linear-dispersion mode exists with

$$\eta_1 = 0$$

$$E = -p_x$$

$$\eta_2(y) = \exp\left[-\int_0^y dy' m(y')\right]$$

Consequences for electronic transport II

This mode survives if the line is curved:

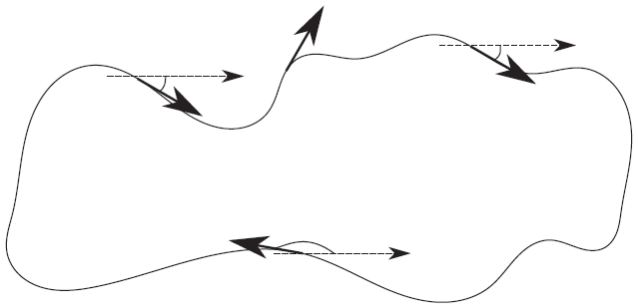

$$\{x, y\} = \mathbf{R}(\tau) \quad |\mathbf{R}'(\tau)| = 1$$

$$\{x, y\} = \mathbf{R}(\tau) + \xi \mathbf{n}(\tau)$$

$$\hat{H} = \frac{\boldsymbol{\sigma}\mathbf{R}'(\tau)}{1 - \xi k(\tau)}\hat{p}_\tau - i\boldsymbol{\sigma}\mathbf{n}(\tau)\frac{\partial}{\partial \xi} + \sigma_z m - \frac{ik\boldsymbol{\sigma}\mathbf{n}(\tau)}{2[1 - \xi k(\tau)]} - \frac{i\boldsymbol{\sigma}\mathbf{R}'(\tau)\xi k'(\tau)}{2[1 - \xi k(\tau)]^2}$$

k is curvature

Tunneling between two lines:

Probability is proportional to

$$\exp\left[-\int_{a_1}^{a_2} |m(y)| dy\right]$$

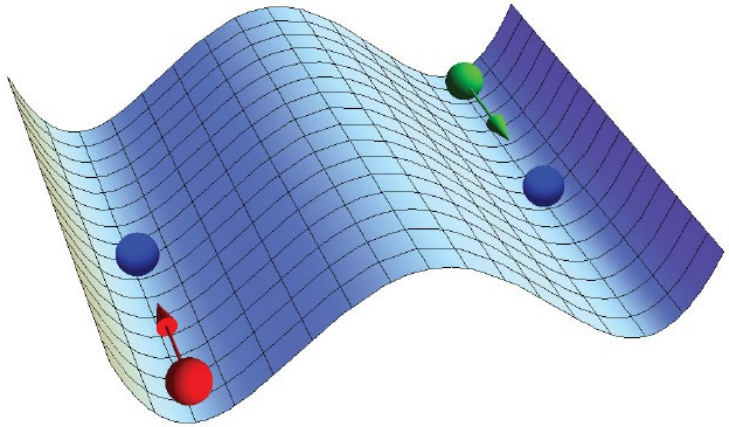

Consequences for electronic transport III

Model of percolation along zero-mass lines

Valid if the distance between lines is larger than typical $\hbar/mv$ and tunneling is negligible

PRL 113, 096801 (2014) PHYSICAL REVIEW LETTERS week ending 29 AUGUST 2014

Metal-Insulator Transition in Graphene on Boron Nitride

M. Titov and M. I. Katsnelson

Landauer formula $$G = \frac{2e^2}{h}\langle N_{line}\rangle$$

Exact result for 2D percolation (Cardy) $$\langle N_{line}\rangle = \frac{\sqrt{3}}{2}\frac{L_x}{L_y}$$

Exact minimal conductivity in percolation model $$\sigma = \sqrt{3}\frac{e^2}{h}$$

$$\exp\langle \ln(L_{\text{line}}/L)\rangle = c(L/\xi')^{3/4}, \qquad \xi' = \sqrt{3}\xi/2$$

$$\langle N_{\text{line}}\rangle = \frac{\sqrt{3}W}{2L}\exp\left[-\frac{(p-1/2)^2}{p_0^2}\right],$$

where $p_0 = c(\xi'/L)^{3/4}$ with $c \approx 0.7$ (see Fig. 3).

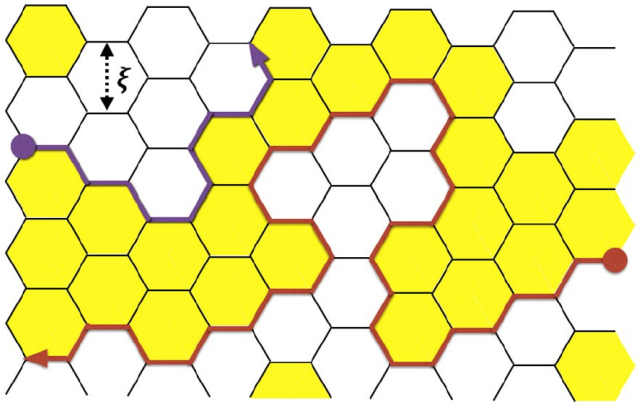

Fractal properties of percolation cluster

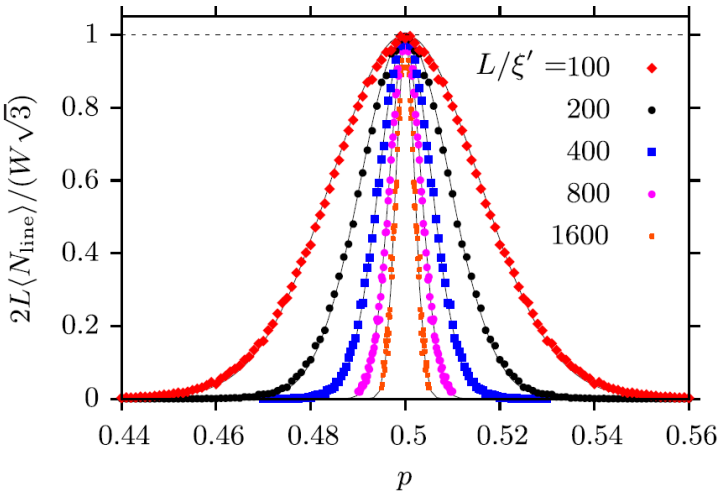

Optical second-harmonic generation

In commensurate phase inversion symmetry in broken due to nonequivalence of sublattices → second-harmonic generation (SHG) is allowed by symmetry

PHYSICAL REVIEW B **99**, 165432 (2019)

Resonant optical second harmonic generation in graphene-based heterostructures

M. Vandelli,[1,2] M. I. Katsnelson,[1,3] and E. A. Stepanov[1,3]

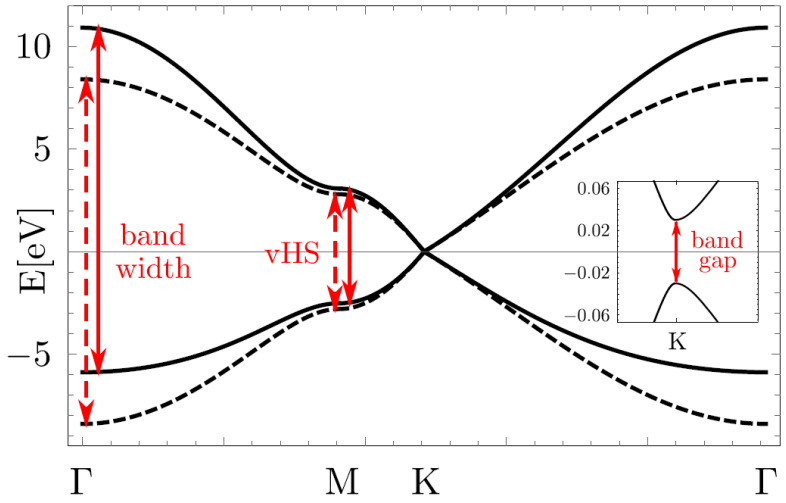

FIG. 1. Dispersion relation of graphene with (solid line) and without (dashed line) account for the next-nearest-neighbor hopping process t'. Red arrows show optical resonances at the bandwidth (Γ point), van Hove singularity (M point), and band gap (K point).

$$t = -2.8 \text{ eV}, t' = -0.1t \quad m = 30 \text{ meV}$$

Electron-hole symmetry should be also broken → either final doping or NNN hopping t'

$$\hat{H}_{ij}[A] = \hat{H}_{ij} \exp\left(-i\frac{e}{c}\int_{\mathbf{R}_i}^{\mathbf{R}_j} \mathbf{A}(\mathbf{r},t)\cdot d\mathbf{r}\right)$$

Contributions to nonlinear optical conductivity

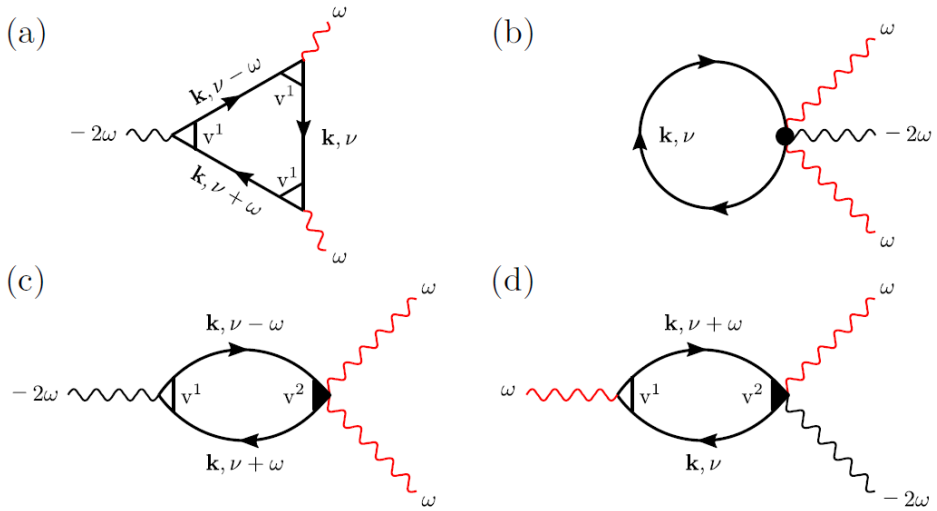

Optical second-harmonic generation II

Analytic expressions

$$j_{\alpha\omega}[A] - j_{\alpha\omega}[0] = \sum_{\beta,\omega'} \left.\frac{\delta j_{\alpha\omega}[A]}{\delta A_{\beta\omega'}}\right|_{A=0} A_{\beta\omega'} + \frac{1}{2}\sum_{\beta\gamma,\omega'\omega''} \left.\frac{\delta^2 j_{\alpha\omega}[A]}{\delta A_{\beta\omega'}\delta A_{\gamma\omega''}}\right|_{A=0} A_{\beta\omega'}A_{\gamma\omega''}$$

$$\left.\frac{\delta^2 j_{\alpha\omega}[A]}{\delta A_{\beta\omega'}\delta A_{\gamma\omega''}}\right|_{A=0} = \left.\frac{\delta^3 \mathcal{F}[A]}{\delta A_{\alpha\omega}A_{\beta\omega'}\delta A_{\gamma\omega''}}\right|_{A=0} = 2e^3\Pi^{\omega\omega'\omega''}_{\alpha\beta\gamma}$$

$$\Pi^{(2)}_{\alpha\beta\delta}(\omega) = \mathrm{Tr}\sum_{\mathbf{k},\nu} \hat{\mathrm{v}}^{(2)}_{\alpha\beta}\hat{G}(\mathbf{k},\nu-\omega)\mathrm{v}^{(1)}_{\delta}\hat{G}(\mathbf{k},\nu+\omega) + 2\,\mathrm{Tr}\sum_{\mathbf{k},\nu}\hat{\mathrm{v}}^{(2)}_{\alpha\beta}\,\hat{G}(\mathbf{k},\nu+\omega)\,\hat{\mathrm{v}}^{(1)}_{\gamma}\,\hat{G}(\mathbf{k},\nu),$$

$$\hat{G}(\mathbf{k},\nu) = [\mathbb{1}(i\nu+\mu) - \hat{H}_{\mathbf{k}}]^{-1}$$

$$\Pi^{(3)}_{\alpha\beta\gamma}(\omega) = \mathrm{Tr}\sum_{\mathbf{k},\nu}\hat{\mathrm{v}}^{(1)}_{\alpha}\hat{G}(\mathbf{k},\nu+\omega)\hat{\mathrm{v}}^{(1)}_{\beta}\hat{G}(\mathbf{k},\nu)\hat{\mathrm{v}}^{(1)}_{\gamma}\hat{G}(\mathbf{k},\nu-\omega)$$

$$\hat{\mathrm{v}}^{(1)}_{\alpha} = \frac{1}{e}\left.\frac{\delta\hat{H}_{\mathbf{k}}[A]}{\delta A_{\alpha}}\right|_{A=0}, \qquad \hat{\mathrm{v}}^{(2)}_{\alpha\beta} = \frac{1}{e^2}\left.\frac{\delta^2\hat{H}_{\mathbf{k}}[A]}{\delta A_{\alpha}\delta A_{\beta}}\right|_{A=0}$$

$$\mathrm{v}^{(1)}_{x}(\mathbf{k}) = \begin{pmatrix} \mathrm{v}^{(1)\,AA}_{x}(\mathbf{k}) & -\sqrt{3}ta\,e^{\frac{-ik_ya}{2}}\sin\left(\frac{\sqrt{3}k_xa}{2}\right) \\ -\sqrt{3}ta\,e^{\frac{+ik_ya}{2}}\sin\left(\frac{\sqrt{3}k_xa}{2}\right) & \mathrm{v}^{(1)\,BB}_{x}(\mathbf{k}) \end{pmatrix},$$

$$\mathrm{v}^{(2)}_{xx}(\mathbf{k}) = \begin{pmatrix} \mathrm{v}^{(2)\,AA}_{xx}(\mathbf{k}) & -\frac{3ta^2}{2}e^{-\frac{ik_ya}{2}}\cos\left(\frac{\sqrt{3}k_xa}{2}\right) \\ -\frac{3ta^2}{2}e^{\frac{ik_ya}{2}}\cos\left(\frac{\sqrt{3}k_xa}{2}\right) & \mathrm{v}^{(2)\,BB}_{xx}(\mathbf{k}) \end{pmatrix},$$

$$\mathrm{v}^{(1)}_{y}(\mathbf{k}) = \begin{pmatrix} -6t'a\cos\left(\frac{\sqrt{3}}{2}k_xa\right)\sin\left(\frac{3}{2}k_ya\right) & -3ita\,e^{-\frac{ik_ya}{2}}\cos\left(\frac{\sqrt{3}}{2}k_xa\right) \\ 3ita\,e^{\frac{ik_ya}{2}}\cos\left(\frac{\sqrt{3}}{2}k_xa\right) & -6t'a\cos\left(\frac{\sqrt{3}}{2}k_xa\right)\sin\left(\frac{3}{2}k_ya\right) \end{pmatrix}$$

$$\mathrm{v}^{(2)}_{yy}(\mathbf{k}) = \begin{pmatrix} -9t'a^2\cos\left(\frac{\sqrt{3}k_x}{2}\right)\cos\left(\frac{3k_y}{2}\right) & -\frac{1}{2}e^{-\frac{1}{2}(ik_y)}t\left(\cos\left(\frac{\sqrt{3}k_x}{2}\right)+8e^{\frac{3ik_y}{2}}\right) \\ -\frac{1}{2}e^{-ik_y}t\left(e^{\frac{3ik_y}{2}}\cos\left(\frac{\sqrt{3}k_x}{2}\right)+8\right) & -9t'a^2\cos\left(\frac{\sqrt{3}k_x}{2}\right)\cos\left(\frac{3k_y}{2}\right) \end{pmatrix}$$

$$\mathrm{v}^{(1)\,AA}_{x}(\mathbf{k}) = \mathrm{v}^{(1)\,BB}_{x}(\mathbf{k}) = -2\sqrt{3}t'a(\sin(\sqrt{3}k_xa) + \sin(\tfrac{\sqrt{3}}{2}k_xa)\cos(\tfrac{3}{2}k_ya))$$

$$\mathrm{v}^{(2)\,AA}_{xx}(\mathbf{k}) = \mathrm{v}^{(2)\,BB}_{xx}(\mathbf{k}) = -3t'a^2(\cos\left(\frac{\sqrt{3}k_xa}{2}\right)\cos\left(\frac{3k_ya}{2}\right) + 2\cos\left(\sqrt{3}k_xa\right))$$

Optical SHG III

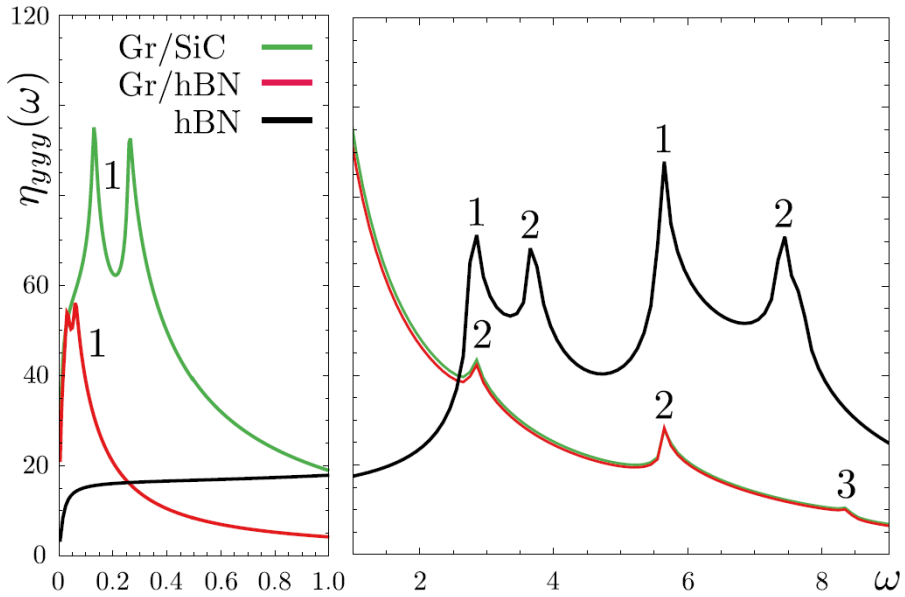

FIG. 3. The absolute value of $\eta_{yyy}(\omega)$ for hBN (black line), Gr/SiC (green line), and Gr/hBN (red line) at low (left) and high (right) frequency ω. The data for Gr/SiC on the right panel is multiplied by a factor of 5 and data for Gr/hBN is multiplied by $5 \times (m_{\mathrm{Gr/SiC}}/m_{\mathrm{Gr/hBN}})$. The data on the left panel is shown without the multiplication. Labels "1," "2," and "3" depict resonances on the band gap, van Hove singularity, and the bandwidth, respectively. The frequency ω of the applied light is given in units of eV.

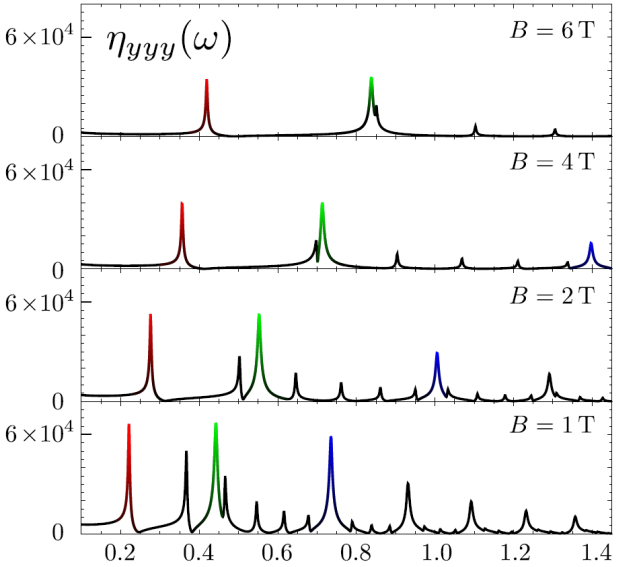

FIG. 5. The absolute value of $\eta_{yyy}(\omega)$ (in a.u.) as the function of the frequency of the applied light ω (in eV) for the case of Gr/SiC under the effect of the magnetic field $B = 1$ T, 2 T, 4 T, and 6 T. Colors serve as guides to the eye and depict resonances on the same Landau levels at different values of the magnetic field.

Optical SHG IV

Direct Observation of Incommensurate–Commensurate Transition in Graphene-hBN Heterostructures via Optical Second Harmonic Generation

E. A. Stepanov,*,† S. V. Semin,† C. R. Woods, M. Vandelli, A. V. Kimel, K. S. Novoselov, and M. I. Katsnelson

Cite This: *ACS Appl. Mater. Interfaces* 2020, 12, 27758–27764 Read Online

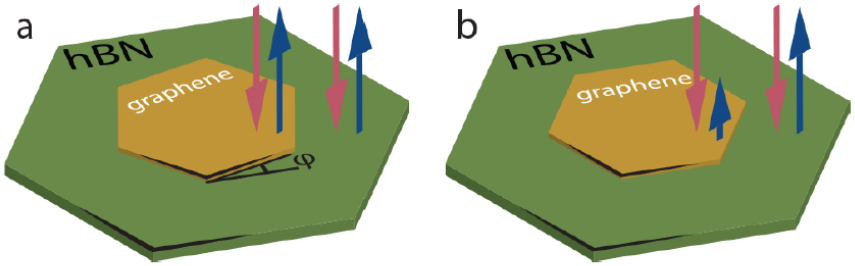

Figure 1. Sketch of the experiment. Green and yellow hexagonal tiles represent hBN and graphene, respectively. Red arrows depict the incident 800 nm light. Blue arrows indicate the SHG response collected at 400 nm from different parts of the sample. (a) In the incommensurate phase, the inversion symmetry of graphene is not broken, and the uniform signal of the SHG comes only from the hBN. (b) After the structural phase transition to the commensurate state, strong modification of the SHG response is observed from the graphene area, where the inversion symmetry breaking is induced by the aligned hBN substrate.

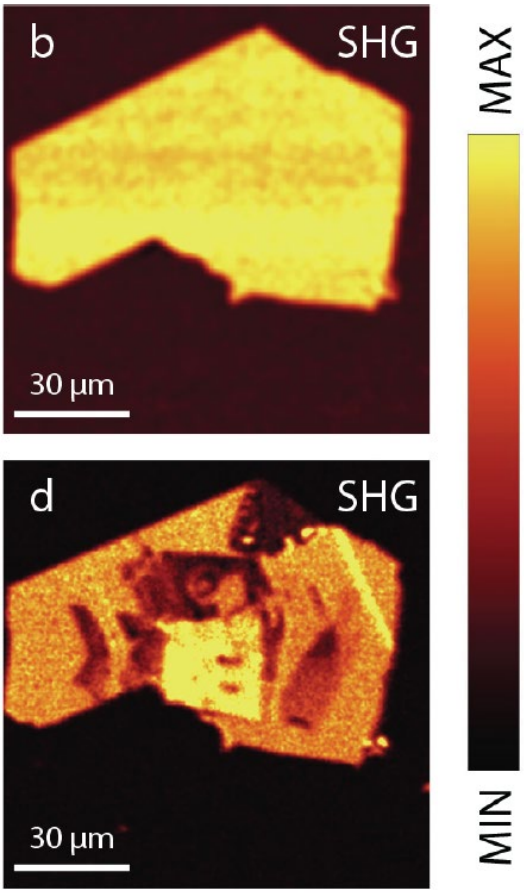

b – incommensurate phase, only hBN signal is visible;
d – commensurate, one can see graphene

Commensurate – incommensurate transition was induced by ieating and clearly detected via SHG

Graphene on graphite

Relaxation of moiré patterns for slightly misaligned identical lattices: graphene on graphite

2D Mater. **2** (2015) 034010

M M van Wijk, A Schuring, M I Katsnelson and A Fasolino

Atomistic simulations: graphene on graphite

Periodicity of moire structure $a_m = \dfrac{a_{\text{lattice}}}{2|\sin(\theta/2)|}$

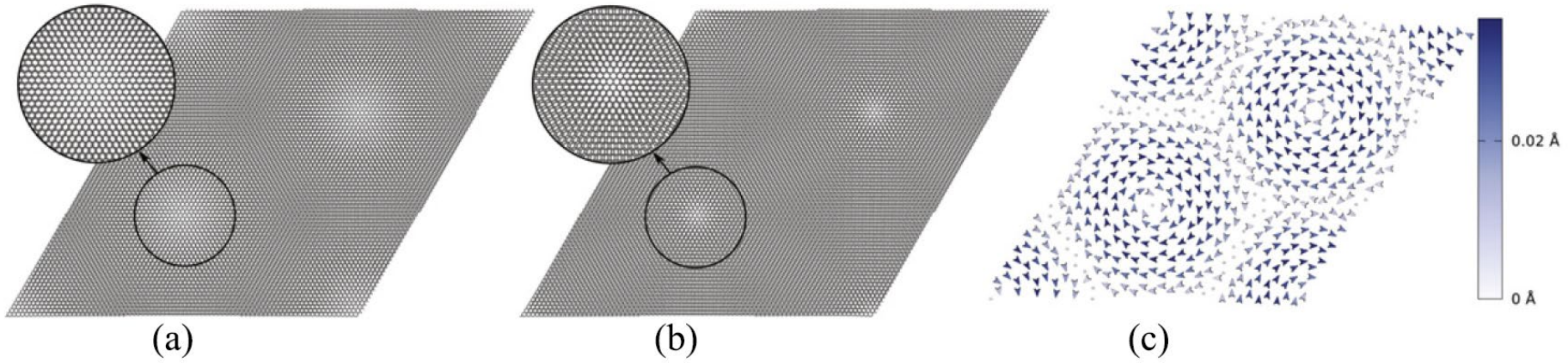

Figure 2. The effects of relaxation are shown for a sample with $(n, m) = (82,1)$, $\theta = 1.2°$ and $a_m = 115.3$ Å. (a) The sample prior to relaxation, (b) the sample after relaxation. Notice the shrinking of the AA stacked area. (c) The displacements of the atoms as the result of relaxation for a sample $(n, m) = (17,1)$, $\theta = 5.7°$ and $a_m = 24.5$ Å. The colour indicates size and the arrow the direction of the displacements.

Graphene on graphite II

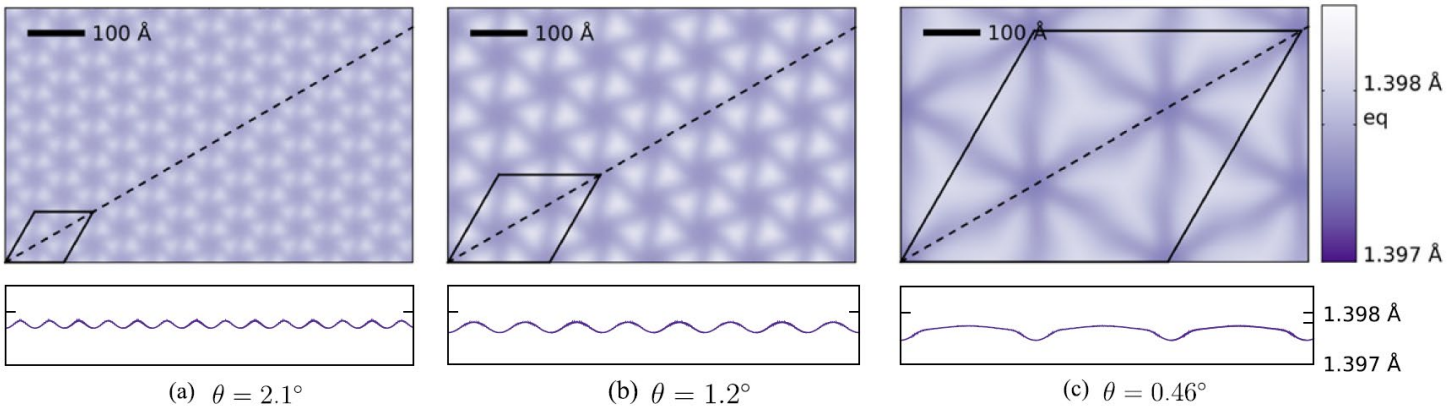

Figure 4. Bond lengths of relaxed configurations for samples where the graphene layer is relaxed in all directions. The supercell is shown in black. The bottom panels show the bond length along the dashed diagonal line. (a) $\theta = 2.1°$, $(n, m) = (47,1)$, $a_m = 66.4$ Å. (b) $\theta = 1.2°$, $(n, m) = (82,1)$, $a_m = 115.3$ Å. (c) θ=0.46°, $(n, m) = (216,1)$, $a_m = 302.6$ Å.

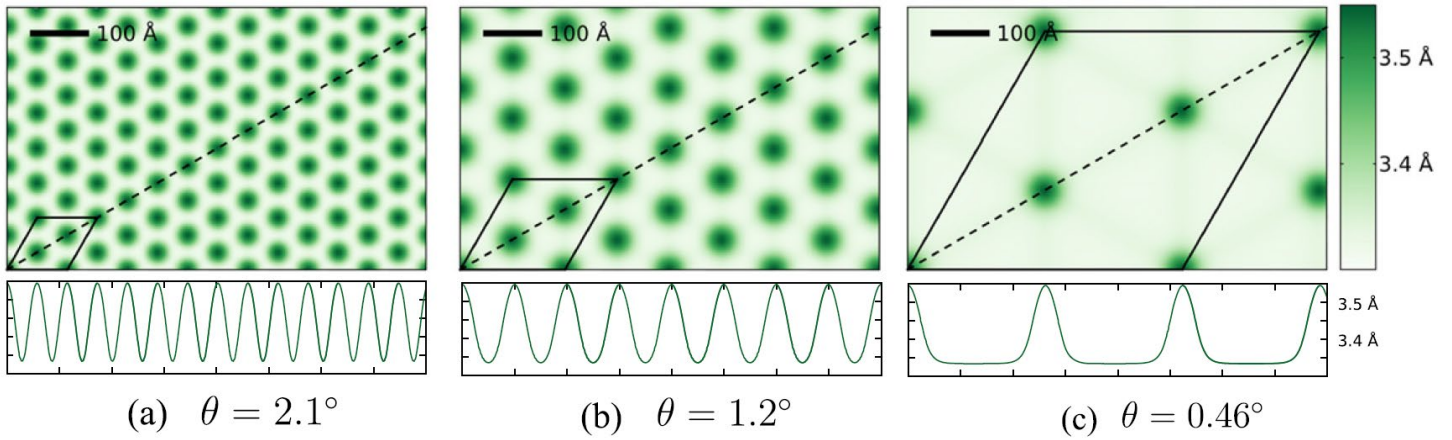

Figure 6. Out-of-plane distance for samples where the graphene layer is relaxed in all dimensions. The bottom panels show the out-of-plane distance along the dashed diagonal line. (a) $\theta = 2.1°$, $(n, m) = (47,1)$, $a_m = 66.4$ Å. (b) $\theta = 1.2°$, $(n, m) = (82,1)$, $a_m = 115.3$ Å. (c) $\theta = 0.46°$, $(n, m) = (216,1)$, $a_m = 302.6$ Å.

Twisted bilayer graphene

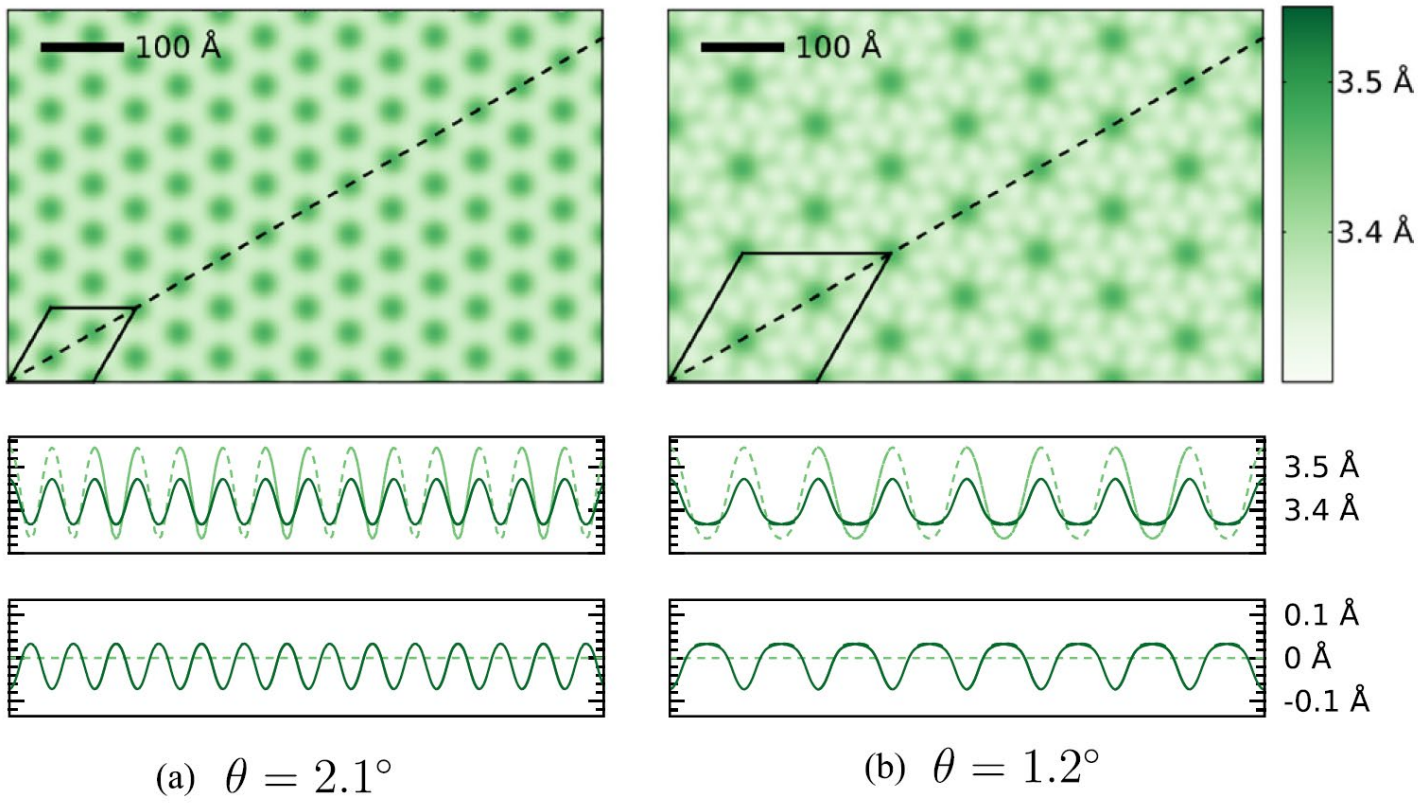

Figure 8. Out-of-plane distance for double layer graphene. The bottom four panels show z along the dashed line in the top figure. The dashed lines show the z for graphene on graphite as in figure 6.

There is a modulation at small angles and some analog of "incommensurability" (small modulations) at larger angles

Description in terms of dislocations

PHYSICAL REVIEW B **102**, 085428 (2020)

Origin of the vortex displacement field in twisted bilayer graphene

Yu. N. Gornostyrev [1,2] and M. I. Katsnelson [3,2]

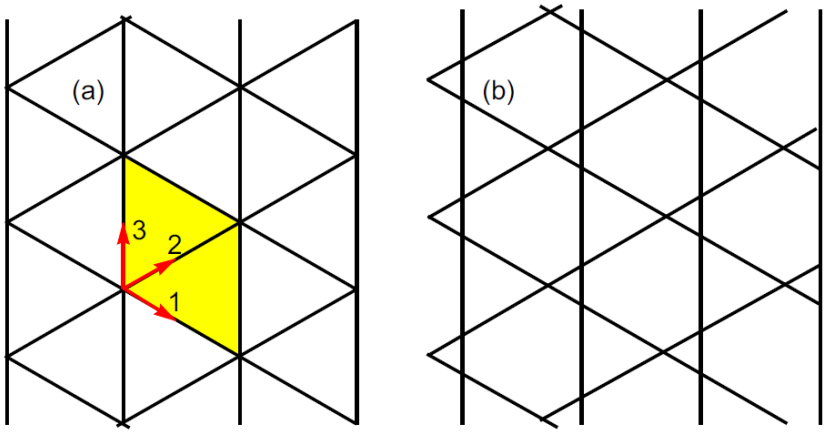

FIG. 1. The schematic representation of the dislocation network used to describe the twist boundary. (a) Network of screw dislocations. (b) Reconstructed network of dislocations. Vectors 1–3 indicate the directions of dislocation lines. The moiré cell is highlighted by a yellow tetragon.

To reproduce vortex structure one can try three families of screw dislocations

Displacement field from individual dislocation is given by analytic formula (Frenkel – Kontorova model)

$$u_s(x) = \frac{b}{\pi}\sum_i \left\{ \arctan\left[\exp\left(\frac{x - x_i^0 - \delta/2}{\xi}\right)\right] + \arctan\left[\exp\left(\frac{x - x_i^0 + \delta/2}{\xi}\right)\right]\right\},$$

δ dislocation core splitting

$\delta \sim \mu b/\gamma$ μ is the shear modulus

γ is the stacking fault energy

Description in terms of dislocations II

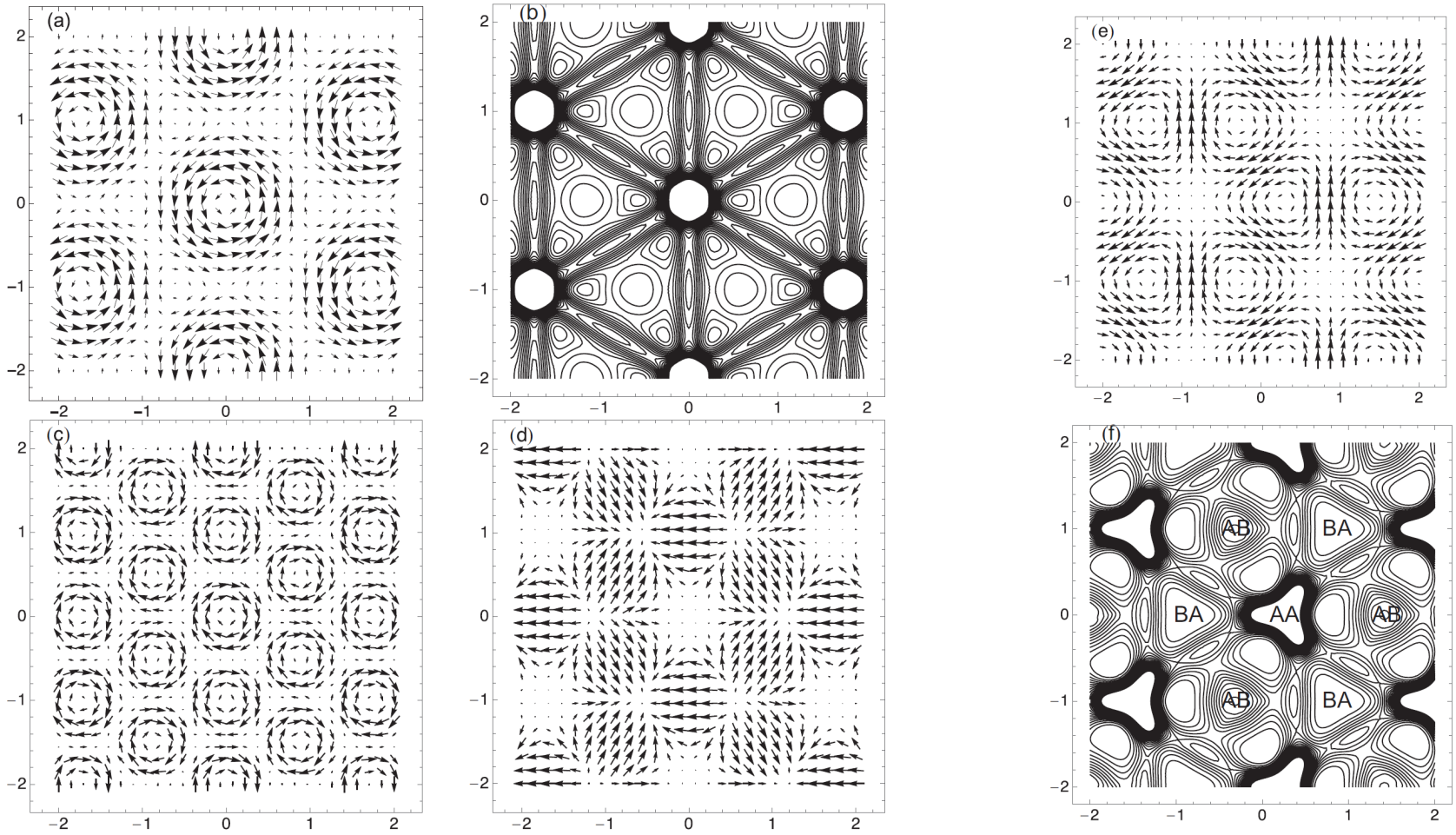

FIG. 3. Displacement $\mathbf{u}_{el}(\mathbf{r})$ shown as a vector field for (a) narrow and (c), (d) split dislocation cores ($\delta = 0.4d$), and (e) for the reconstructed dislocation network. (c) and (d) display screw and edge components of the displacement field, respectively, in the case of split dislocation. (b) and (f) present the distribution of the strain energy density determined by Eq. (9) for cases (a) and (e), respectively. The value ξ is equal $0.05d$ in cases (a)–(c) and $0.15d$ in cases (e) and (f). Distances along the X, Y axes are given in units of $L\sqrt{3}/2$, where L is the separation between the moiré coincidence points.

Description in terms of dislocations III

Pseudomagnetic fields

$$A_x = -2c\beta t u_{xy}.$$

$$A_y = -c\beta t\left(u_{xx} - u_{yy}\right)$$

$$\frac{evB}{c} = \frac{\partial A_y}{\partial x} - \frac{\partial A_x}{\partial y}$$

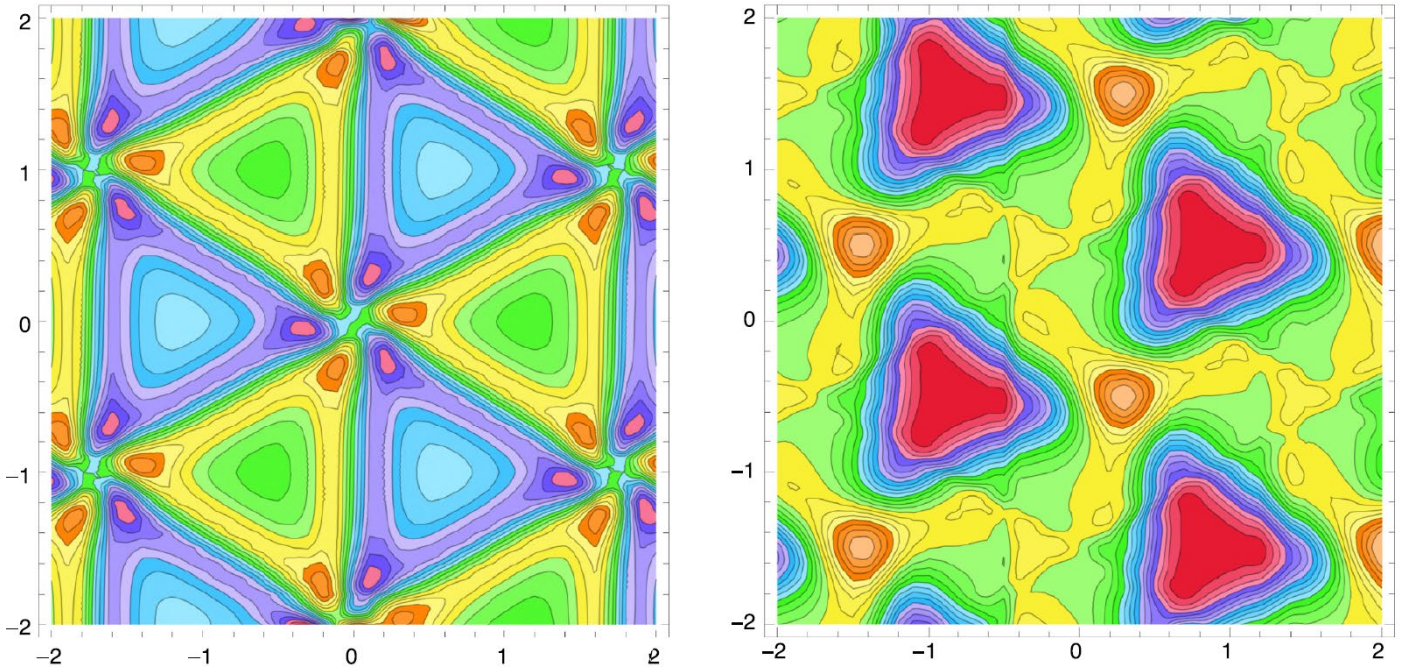

FIG. 5. Distribution of PMF calculated by using Eqs. (10) and (11) for the network of narrow dislocations shown in Fig. 3(a) (left) and for the reconstructed dislocation network shown in Fig. 3(e) (right). Distances along the X, Y axes are given in units of $L\sqrt{3}/2$, where L is the separation between the moiré coincidence points.

There is an analytic formula for pseudomagnetic field, quite cumbersome but explicit

Description in terms of vortices is consistent with that in terms of dislocations

For graphene at hBN one needs to add three families of edge dislocations, due to lattice misfit

Large-scale TB simulations plus experiment

Large-area, periodic, and tunable intrinsic pseudo-magnetic fields in low-angle twisted bilayer graphene

NATURE COMMUNICATIONS | (2020)11:371

Haohao Shi[1,2,6], Zhen Zhan[3,6], Zhikai Qi[4], Kaixiang Huang[3], Edo van Veen[5], Jose Ángel Silva-Guillén[3], Runxiao Zhang[1,2], Pengju Li[1,2], Kun Xie[1,2], Hengxing Ji[4], Mikhail I. Katsnelson[5], Shengjun Yuan[3*], Shengyong Qin[1,2*] & Zhenyu Zhang[1]

Atomic relaxation effects are essential

Electronic properties of TBG with twist angle $\theta = 0.48°$

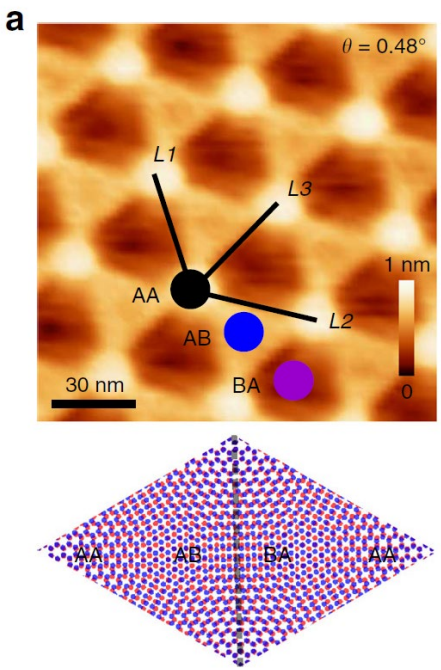

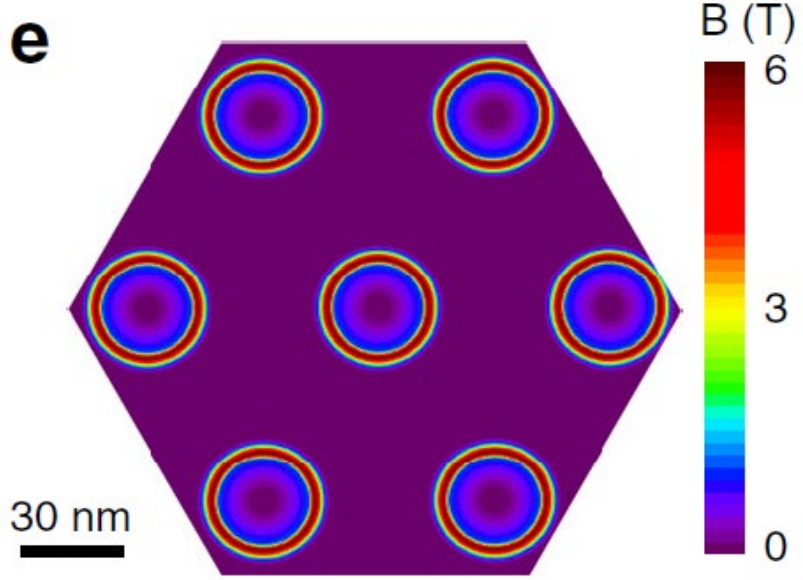

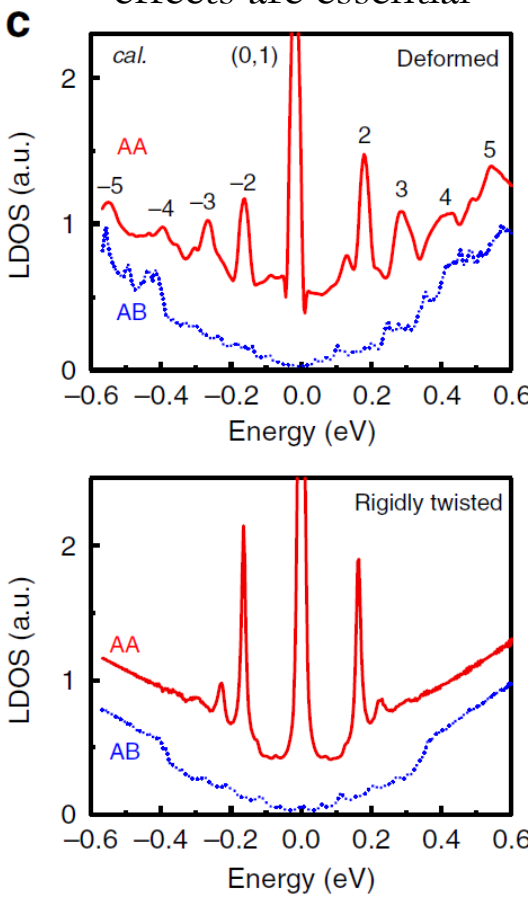

Calculated distribution of pseudomagnetic field

Large-scale TB simulations plus experiment

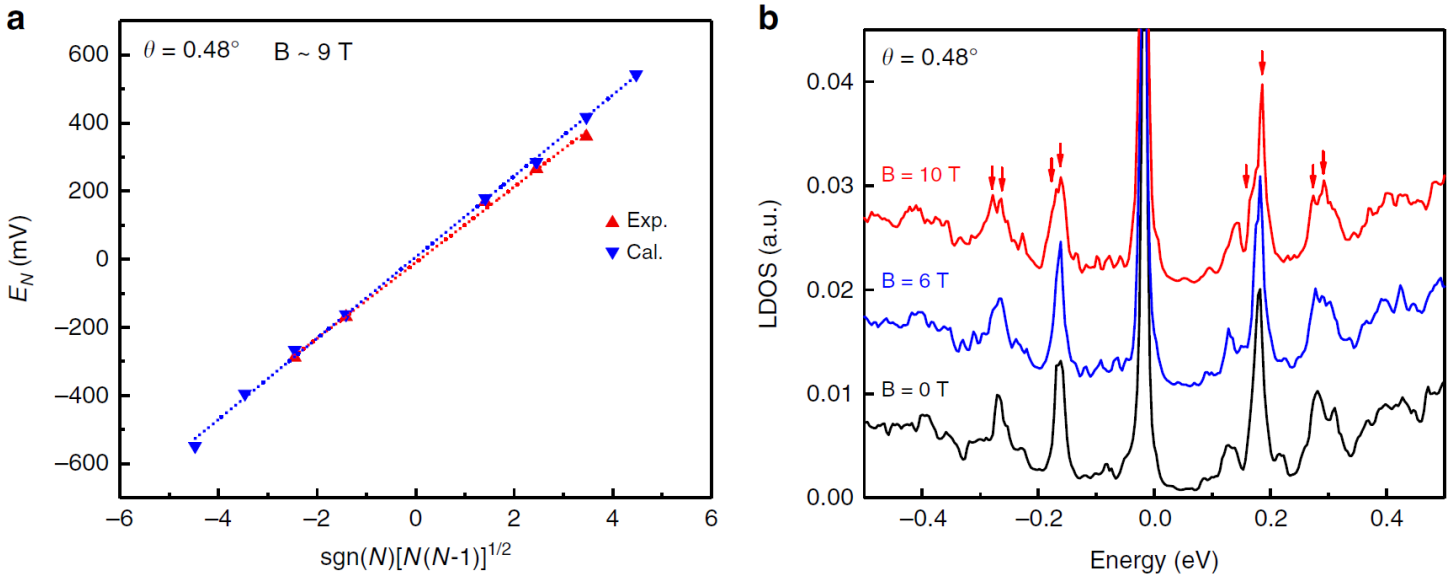

Fig. 2 Pseudo-Landau levels in the deformed twisted bilayer graphene with $\theta = 0.48°$. a Linear fit of the equation $E_N \propto \sqrt{N(N-1)}$ and the obtained pseudo magnetic fields is about 9 T. **b** Calculated LDOS at AA region under the external magnetic fields, in which we can confirm the splittings of the pseudo-Landau level due to the break of the valley degeneracy.

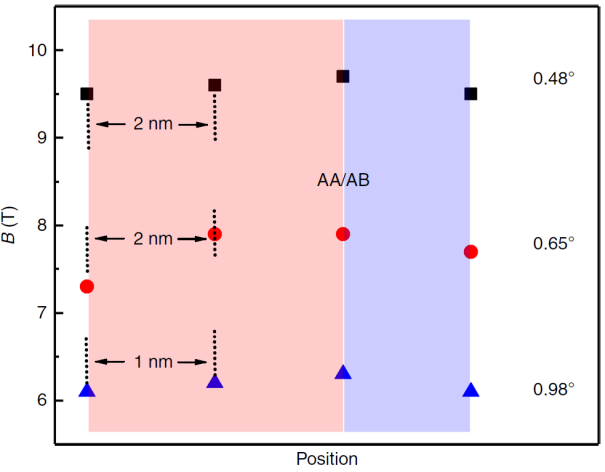

Fig. 5 The fitted pseudo-magnetic field of TBGs with different twisted angles around the region of AA/AB transtion. The obtained PMFs increase with the decreasing twisted angles and the PMF areas are distributed near the AA regions with its maximum value occuring at the AA/AB transitions, which is highly consistent with our calculated results.

Quasicrystals

Unrelaxed moire pattern is periodic if $\cos\theta = \frac{3q^2 - p^2}{3q^2 + p^2}$ with integer p and q

$\theta = 30^\circ$ incommensurate (quasicrystal) structure

Contrary to conventional 3D quasicrystals graphene quasicrystals are easily tunable!

For so large misorientation angle atomic relaxation is negligible and we are always in incommensurate phase

Dodecagonal bilayer graphene quasicrystal and its approximants

Guodong Yu[1,2,3], Zewen Wu[1,3], Zhen Zhan[1], Mikhail I. Katsnelson[2] and Shengjun Yuan[1,2*]

npj Computational Materials (2019)5:122

PHYSICAL REVIEW B **102**, 045113 (2020)

Pressure and electric field dependence of quasicrystalline electronic states in 30° twisted bilayer graphene

Guodong Yu,[1,2,*] Mikhail I. Katsnelson,[2] and Shengjun Yuan[1,2,†]

PHYSICAL REVIEW B **102**, 115123 (2020)

Electronic structure of 30° twisted double bilayer graphene

Guodong Yu,[1,2] Zewen Wu,[1] Zhen Zhan,[1] Mikhail I. Katsnelson,[2] and Shengjun Yuan[1,2,*]

Quasicrystals II

Top view of twisted bilayer graphene for different misorientation angles

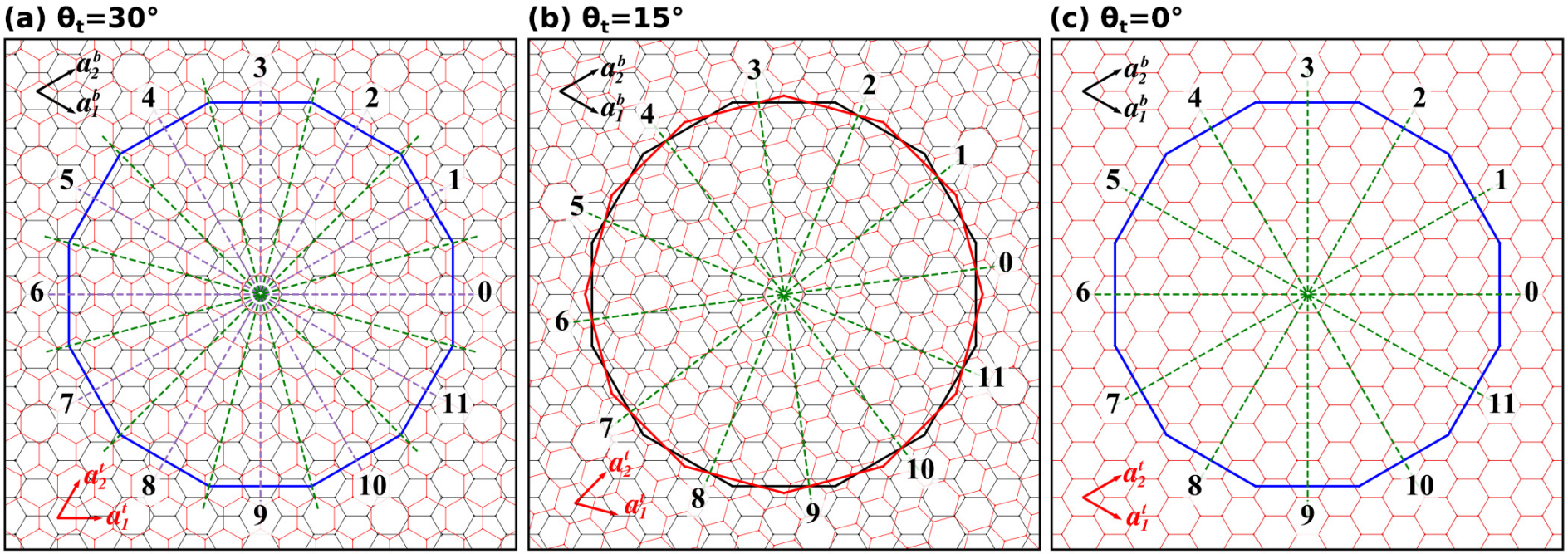

Quasicrystals III

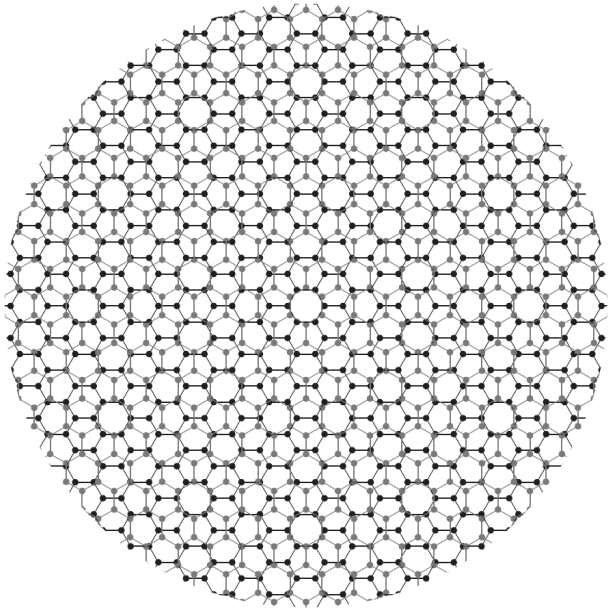

Using approximants to calculate electronic structure; elementary cell is huge but doable via tight-binding propagation method

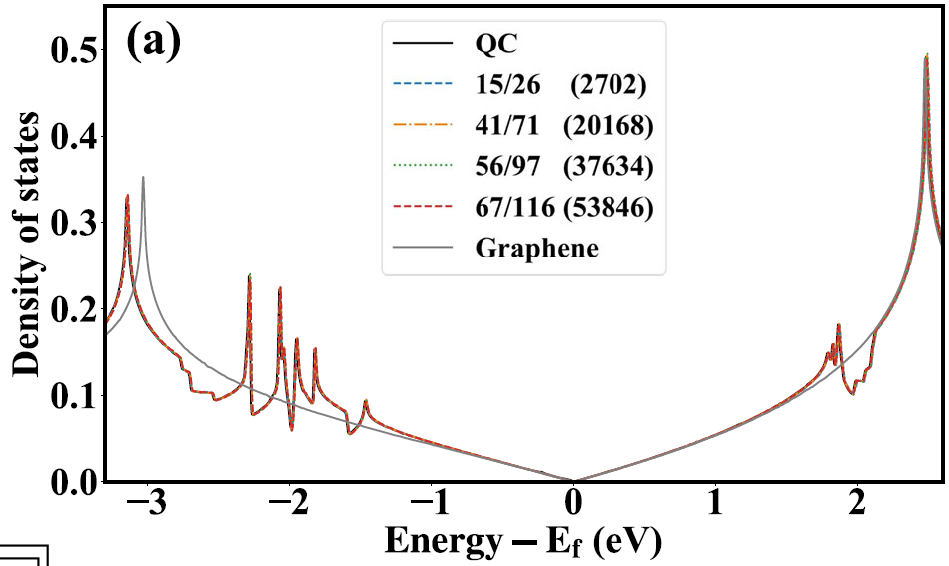

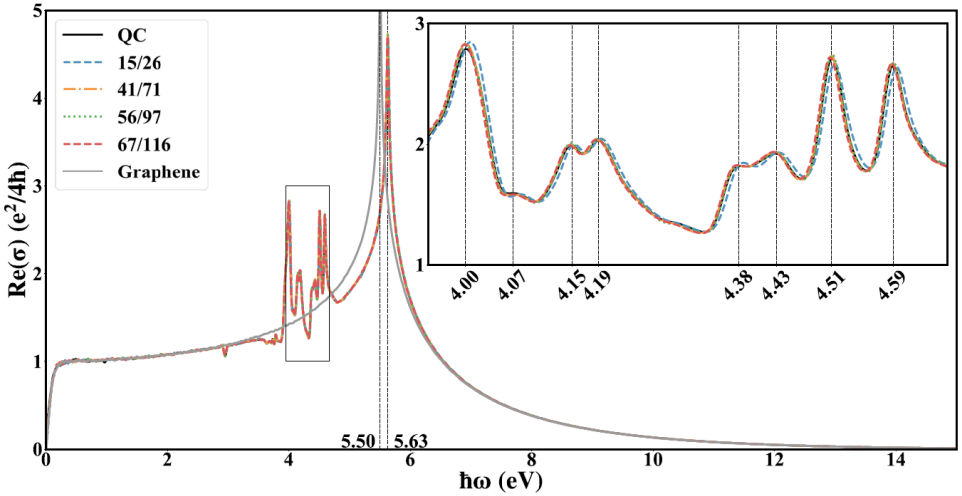

Bright features appear only far enough from the conical point

Quasicrystals IV

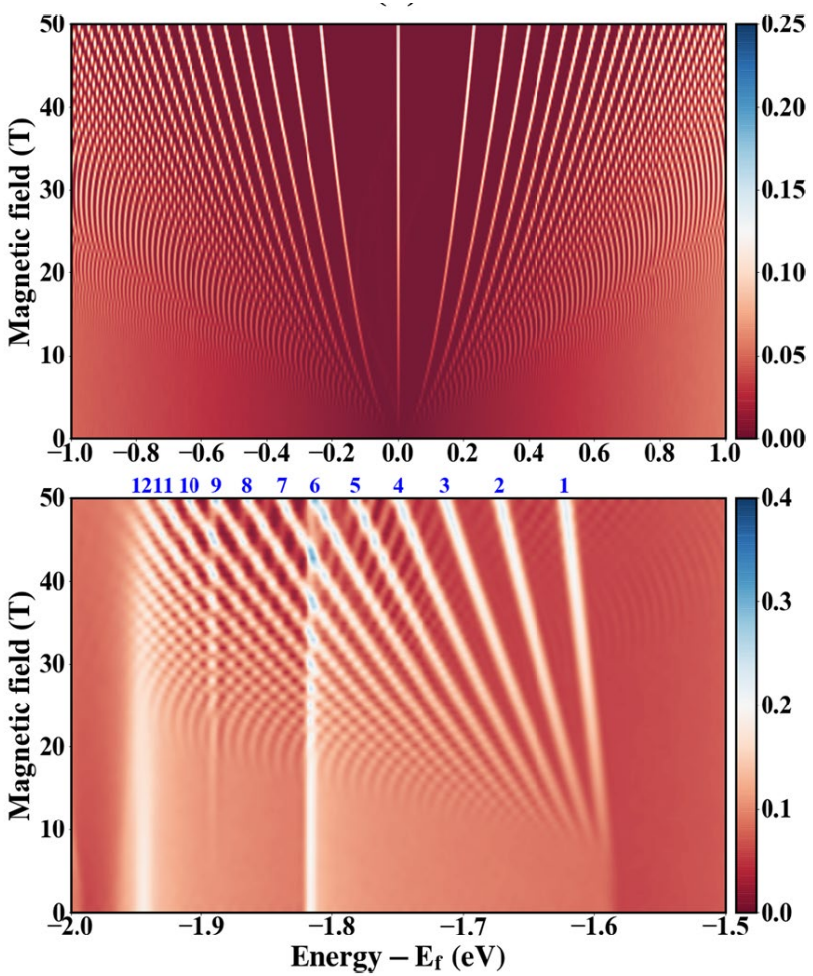

Landau levels (Hofstadter batterfly)

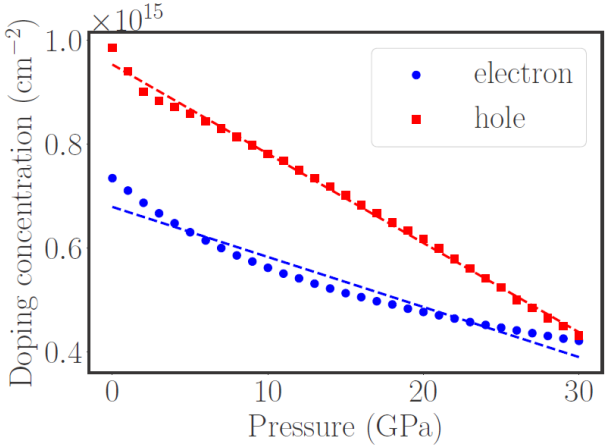

FIG. 5. The concentrations of holes and electrons that are needed to tune the Fermi level to meet the VBM and CBM.

Uniaxial pressure moves the singularities closer to the Fermi energy

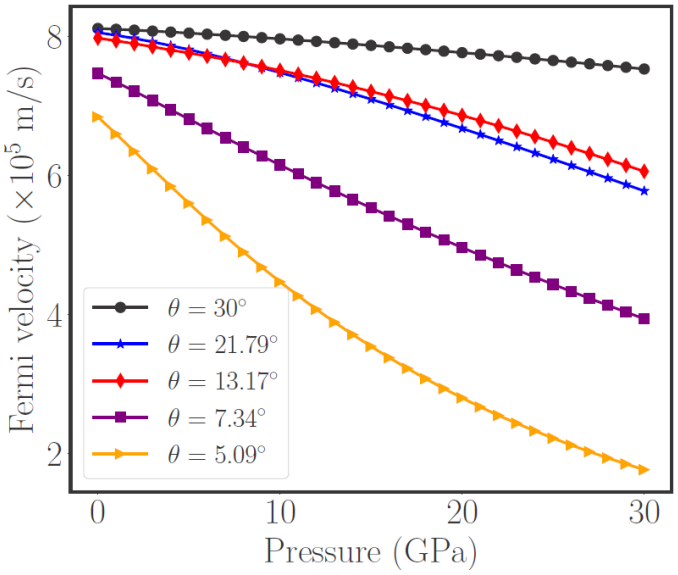

Example of what we are doing: Plasmonic quantum dots

Quantum dot-like plasmonic modes in twisted bilayer graphene supercells

2D Mater. **9** (2022) 014004

Tom Westerhout, Mikhail I Katsnelson and Malte Rösner*

Real-space simulations

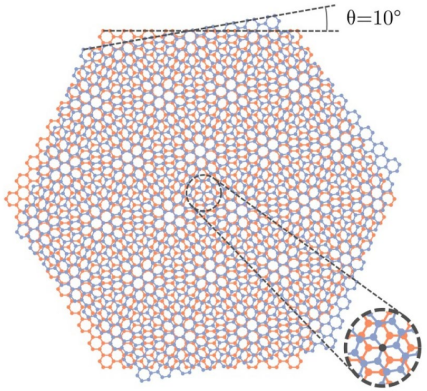

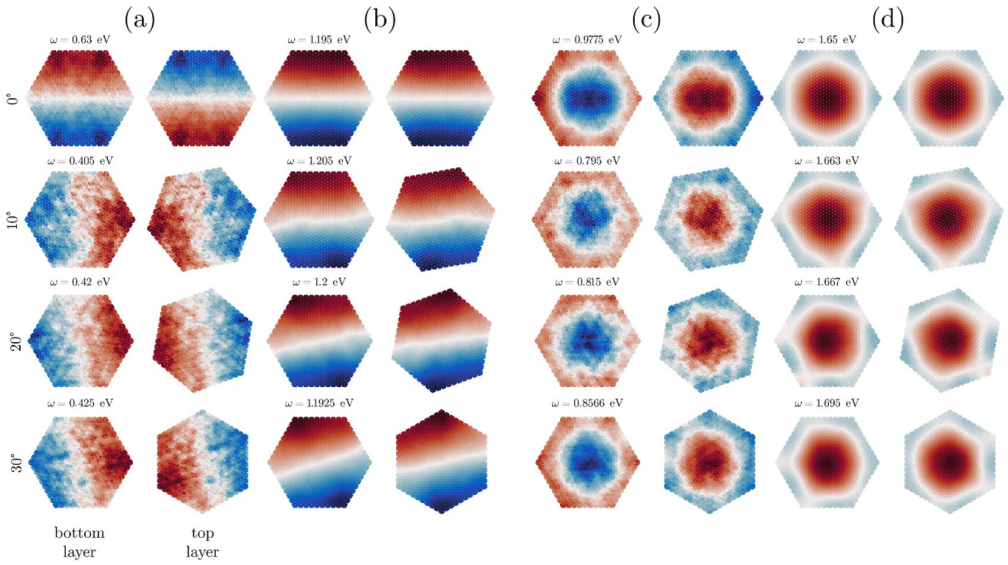

Figure 7. Plasmonic eigenmodes in real space for various twisting angles $\theta = 0°, 10°, 20°, 30°$. Columns show evolution of different modes: (a) 'dark' dipole, (b) 'bright' dipole, (c) 'dark' 1s, (d) 'bright' 1s.

Quantization of plasmon spectrum

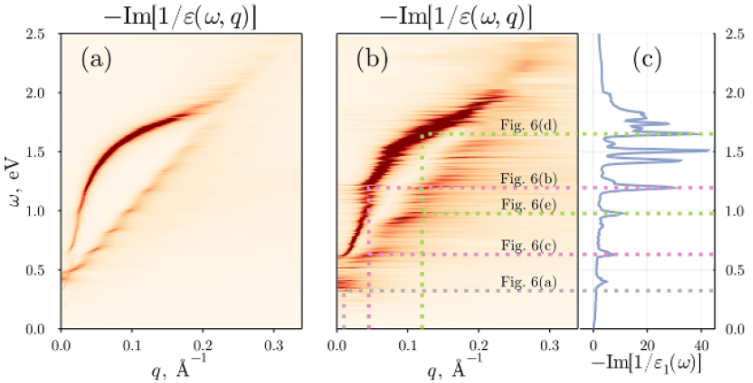

Figure 5. (a) Plasmonic dispersion for a supercell with diameter $d \approx 150$Å (11 028 atoms). (b), (c) Plasmonic dispersion for a supercell with diameter $d \approx 80$ Å (3252 atoms) together with full EELS(ω). Annotations in panel (c) refer to subplots of figure 6.

Examples of plasmonic eigenmodes for different misorientation angles

Main collaborators

Annalisa Fasolino, Merel van Wijk, Guus Slotman, Sasha Rudenko, Malte Rösner, Tom Westerhout (Nijmegen)
Kostya Novoselov (Singapore)
Yuri Gornostyrev (Ekaterinburg)
Evgeny Stepanov (Paris)
Shengjun Yuan and Guodong Yu (Wuhan)

Conclusions

- Atomic relaxation is very important for small enough misorientation angles
- Twisted VdW heterostructures are model systems to study physics of commensurability and incommensurability in condensed matter
- Description in terms of vortices, dislocations and other topological effects may be very suitable
- Second-harmonic generation can be a sensitive experimental tool to study commensurate-incommensurate transition